

**Multi-Modality Image Fusion by Real-Time  
Tracking of Volumetric Brain Deformation During  
Image Guided Neurosurgery**

by

Alida Tei

B.S., Biomedical Engineering,

Worcester Polytechnic Institute, 2000

Submitted to the Department of Electrical Engineering and Computer  
Science

in partial fulfillment of the requirements for the degree of  
Master of Science in Electrical Engineering and Computer Science  
at the

MASSACHUSETTS INSTITUTE OF TECHNOLOGY

February 2002

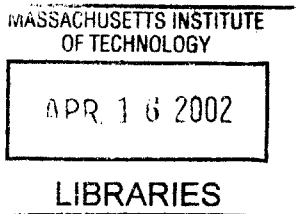
©2002 Massachusetts Institute of Technology. All rights reserved.

Author . . . . .  
Department of Electrical Engineering and Computer Science  
January 18, 2002

Certified by . . . . .  
Simon K. Warfield  
Assistant Professor, Department of Radiology, Harvard Medical  
School and Brigham and Women's Hospital  
Thesis Supervisor

Certified by . . . . .  
William M. Wells  
Research Scientist, MIT AI Laboratory, HST Affiliated Faculty,  
Assistant Professor, Department of Radiology, Harvard Medical  
School and Brigham and Women's Hospital  
Thesis Supervisor

Accepted by . . . . .  
Arthur C. Smith  
Chairman, Department Committee on Graduate Students



**BARKER**

# Multi-Modality Image Fusion by Real-Time Tracking of Volumetric Brain Deformation During Image Guided Neurosurgery

by

Alida Tei

Submitted to the Department of Electrical Engineering and Computer Science  
on January 18, 2002, in partial fulfillment of the  
requirements for the degree of  
Master of Science in Electrical Engineering and Computer Science

## Abstract

This thesis describes a fast method to increase the information-content of intra-operatively acquired images by tracking volumetric brain deformations during neurosurgical procedures. Image Guided Neurosurgery (IGNS) is employed to help surgeons distinguish between healthy and diseased brain tissues, which can have similar visual appearance. High-performance computing algorithms and parallel hardware configurations are the key enabling technologies that allow this method to be quick enough for clinical use.

A finite element based biomechanical model was used during IGNS procedures to capture non-rigid deformations of critical brain structures. These structures, extracted from pre-operative data acquisition, were mapped onto intra-operative Magnetic Resonance (MR) images. This method meets the real-time constraints of neurosurgery and allows for the visualization of multi-modality data, otherwise not available during surgery, together with intra-operative MR data.

Thesis Supervisor: Simon K. Warfield

Title: Assistant Professor, Department of Radiology, Harvard Medical School and Brigham and Women's Hospital

Thesis Supervisor: William M. Wells

Title: Research Scientist, MIT AI Laboratory, HST Affiliated Faculty, Assistant Professor, Department of Radiology, Harvard Medical School and Brigham and Women's Hospital

## Acknowledgments

This thesis summarizes results of the research that I carried out at the Surgical Planning Laboratory (SPL) from June 2001 until January 2002. This work would not have been possible without the main supervision of Simon Warfield, who showed me all the tools and was always very helpful at any time of the day. I would also like to acknowledge Sandy Wells, who first gave me the chance to work at the SPL and who supervised me together with Simon, also giving me all the help I needed to complete my thesis. While Simon and Sandy gave me supervision in engineering and science, all the clinical guidance was provided by Florin Talos, who made me really appreciate how medical imaging fits into neurosurgical practice.

Together with Simon, Sandy and Florin, many other people at the SPL and MIT-AI lab helped and contributed to this work. First, I would like to thank Matthieu Ferrant, who was always ready to help, even from Belgium, and was also a good friend. Then, I would like to acknowledge Aditya Bharatha, who worked close to me during summer and listened to all my frustration. I would like to thank many other people who supported me in different ways, here is a short list (my apologies to those whom I have forgotten): Carl-Fredrik, Albert, Marianna, Karl, Lauren, Delphin, Raul, Peter Black and Eric Grimson.

A very special thanks goes to Ferenc Jolesz and Ron Kikinis, who both make this kind of research possible and lead the way for clinically valuable image processing. Along with the support with my research issues, I would like to thank Walter Rosenblith, who provided me with financial support through a fellowship for my first 12 months at MIT, and Ferenc Jolesz, who granted me a research assistantship for the last semester.

Hopefully I have not disappointed any of the people I just mentioned. I truly am very grateful to them, as they have supported me in many ways. Lastly, I would like to thank those who have given me the moral support I needed to finish my Master's Degree: my boyfriend Alberto, my family, and all my friends in Italy and in the States.

## Biographical Note and Publications

I am a second year graduate student at the *Massachusetts Institute of Technology* in the Electrical Engineering and Computer Science department, as well as a *Master of Science Degree* candidate, and expect to graduate in February 2002. Previously, I attended my undergraduate studies at the *Worcester Polytechnic Institute*, where I obtained a *Bachelor of Science* degree in Biomedical Engineering (with concentration in Electrical Engineering and a minor in Computer Science) with High Distinction in May 2000.

I was born in Ivrea, Italy, and lived there until age 15, when I moved to Zug, Switzerland, to finish my high-school studies at the *Institut Montana*, an international boarding school, where I graduated in July 1996 with the highest score. I developed interest in medical image processing during my undergraduate years, both while I was doing my internship in my junior year, and while I was working on my final undergraduate project.

In the making of this thesis, I published some work both as an author and as a co-author as follows:

- Alida Tei, Florin Talos, Aditya Bharatha, Matthieu Ferrant, Peter McL. Black, Ferenc A. Jolesz, Ron Kikinis, and Simon K. Warfield. Tracking Volumetric Brain Deformation During Image Guided Neurosurgery. In *VISIM: Information Retrieval and Exploration in Large Medical Image Collections*, in conjunction with *MICCAI 2001: the Fourth International Conference on Medical Image Computing and Computer-Assisted Intervention, Oct 14-18, Utrecht, The Netherlands*, Springer-Verlag, Heidelberg, Germany, 2001. [39]
- Simon K. Warfield, Florin Talos, Alida Tei, Aditya Bharatha, Arya Nabavi, Matthieu Ferrant, Peter McL. Black, Ferenc A. Jolesz, and Ron Kikinis. Real-Time Registration of Volumetric Brain MRI by Biomechanical Simulation of Deformation during Image Guided Neurosurgery. In *Computing and Visualization in Science*, Springer-Verlag, Heidelberg, Germany, 2002. In Press. [45]

- Simon K. Warfield, Alexandre Guimond, Alexis Roche, Aditya Bharatha, Alida Tei, Florin Talos, Jan Rexilius, Juan Ruiz-Alzola, Carl-Fredrik Westin, Steven Haker, Sigurd Angenent, Allen Tannenbaum, Ferenc A. Jolesz, and Ron Kikinis. Advanced Nonrigid Registration Algorithms for Image Fusion. In Arthr W. Toga, editor, *Brain Mapping: The Methods*. San Diego, USA: Academic Press, 2nd edition, 2002. In Press. [42]

The first publication was accompanied by an oral presentation at the *VISIM* workshop, held in conjunction with the *MICCAI 2001* conference. The second publication has been accepted and will appear in *Computing and Visualization in Science* early this year. The third publication is a chapter of the book *Brain Mapping: The Methods*, which is also in press.

# Contents

<b>1</b>	<b>Introduction</b>	<b>14</b>
1.1	Context of the work . . . . .	14
1.2	Image Guided Neurosurgery (IGNS) . . . . .	15
1.3	Multi-Modality Image Fusion for IGNS . . . . .	17
1.4	Non-Rigid Registration for IGNS . . . . .	18
1.5	Previous Related Work . . . . .	20
1.6	Organization of Thesis Document . . . . .	23
<b>2</b>	<b>Intra-Operative Methodology: Segmentation and Rigid Registration</b>	<b>25</b>
2.1	Methodology Overview . . . . .	25
2.1.1	Pre-Operative Imaging . . . . .	27
2.1.2	Intra-Operative Imaging . . . . .	28
2.2	Intra-Operative Segmentation and Rigid Registration . . . . .	28
2.2.1	Motivation . . . . .	28
2.2.2	Segmentation of Intra-Operative Images . . . . .	28
2.2.3	Affine Registration of Pre- to Intra-Operative Images . . . . .	29
2.2.4	Discussion . . . . .	30
2.3	Intra-Operative Segmentation and Rigid Registration: an Alternative Approach . . . . .	30
2.3.1	Motivation . . . . .	30
2.3.2	Rigid Registration of Pre- to Intra-Operative Images . . . . .	30
2.3.3	Segmentation of Intra-Operative Images . . . . .	31

2.3.4	Discussion . . . . .	32
<b>3</b>	<b>Intra-Operative Methodology: Non-Rigid Registration</b>	<b>33</b>
3.1	Finite Element Modeling of Elastic Membranes and Volumes . . . . .	34
3.2	Mesh Generation . . . . .	38
3.3	Active Surface Deformation . . . . .	39
3.4	Biomechanical Volumetric Deformation . . . . .	41
3.5	Application of Volumetric Deformation Fields to Image Data . . . . .	42
3.6	HPC Implementation . . . . .	43
<b>4</b>	<b>Intra-Operative Methodology: Visualization</b>	<b>45</b>
4.1	Multi-Modality Image Fusion . . . . .	47
4.2	Intra-Operative Navigation . . . . .	48
<b>5</b>	<b>Deformable Atlas-based Tracking of Critical Brain Structures during IGNS</b>	<b>50</b>
5.1	Motivation . . . . .	50
5.2	Description . . . . .	51
5.3	Results . . . . .	54
<b>6</b>	<b>Tracking of Vascular Structures during IGNS</b>	<b>60</b>
6.1	Motivation . . . . .	60
6.2	Description . . . . .	61
6.3	Results . . . . .	63
<b>7</b>	<b>Tracking of Cortical Structures during IGNS</b>	<b>66</b>
7.1	Motivation . . . . .	66
7.2	Description . . . . .	67
7.3	Results . . . . .	69
<b>8</b>	<b>Conclusions and Future Work</b>	<b>74</b>
8.1	Discussion of Results . . . . .	74
8.2	Major Achievements and Contributions . . . . .	75

8.3 Perspectives and Future Work . . . . .	76
<b>A Glossary of Abbreviations</b>	<b>78</b>
<b>B Computational Facilities at the Surgical Planning Laboratory</b>	<b>79</b>



# List of Figures

1-1	Open Magnet MR configuration in the MRT room at the BWH. . . .	16
1-2	Intra-operative MR images. Left: initial image, acquired before skin incision. Center: first intra-operative imaging update, acquired after skin incision. Right: second intra-operative imaging update, acquired after performing some degree of resection. . . . .	19
1-3	Intra-operative MR images. Left: initial image, acquired before skin incision. Center: first intra-operative imaging update, acquired after skin incision. Right: second intra-operative imaging update, acquired after performing some degree of resection. Upper slices show a region near the lesion. Lower slices show that, even away from the lesion, the brain shift is very pronounced. . . . .	19
2-1	Schema for intra-operative segmentation and registration. . . . .	27
3-1	Schema of the deformable registration algorithm illustrating the matching of an input image onto a target image. . . . .	34
4-1	Screen shots of the 3D Slicer. . . . .	46
4-2	Multi-modality image fusion: Surface models of brain (white) and residual tumor (green), generated from an intra-operative image acquired after some degree of resection, are shown together with surface models of arteries (red) and veins (blue), generated from pre-operative MRA data. . . . .	47

4-3	Intra-operative navigation: Surface models of the brain (white), the ventricles (blue), the corticospinal tract (red) and the tumor (green), generated from pre-operative and intra-operative data, are displayed aligned with an intra-operative SPGR scan and together with the virtual surgical instrument tracked in the coordinate system of the patient's image acquisition. . . . .	49
5-1	Head muscles (top) and central nervous system structures (bottom) of the generic brain atlas used for intra-operative matching. . . . .	52
5-2	Top: Visual system extracted from the generic brain atlas used for intra-operative matching. Bottom: Image of structures such as corticospinal tract and optic radiation, which were needed for neurosurgical cases, and were therefore extracted from the generic atlas. . . . .	53
5-3	Post-resection models of the brain (white), the ventricles (blue), the tumor (green) and the optic radiation (yellow). The tumor is clearly located next to the optic radiation. After most of the resection, the brain has shifted significantly. In the bottom images, the models are shown along with the intra-operatively acquired MR dataset. . . . .	55
5-4	Intra-operative MR dataset aligned with the corticospinal tract extracted from the deformed atlas, displayed with the virtual surgical needle, interactively tracked within the patient's coordinate system. . . . .	56
5-5	Pre- (left) and post-resection (right) models of the brain (white), the ventricles (blue) and the corticospinal tract (pink). The top images present only models of the brain, where the brain shift is very pronounced. The bottom images show the same views with all other models, here it is evident that the tumor was located next to the corticospinal tract. . . . .	57

5-6	Visualization of surface (top) and volumetric deformation fields (middle and bottom) of the first intra-operative scan volume onto the second intra-operative scan volume of the second case. In the bottom images, the volumetric deformation fields are shown aligned with the corticospinal tract (blue). The color-coding indicates the magnitude of the deformation at every point on the surface or cuts of the deformed volume, and arrows indicate the magnitude and direction of the deformation. . . . .	58
6-1	Models of arteries (red) and veins (blue) rigidly registered to the pre-operative SPGR scan (shown in the bottom figure). . . . .	62
6-2	Models of arteries (red) and veins (blue) deformed onto an intra-operative SPGR image acquired after some degree of resection and also shown in the picture. Note that the arteries in proximity of the resection cavity overlap with the flow voids present in the intra-operative MR image. . . . .	64
7-1	Top: Models of the brain (white), the ventricles (blue), the tumor (green), and the fMRI activation areas (red) extracted from the pre-operative fMRI scan. Bottom: Models of the tumor and fMRI activation areas shown along with the pre-surgical SPGR image provide a closer look at the region near the tumor. The strong anatomical relationship of the tumor and the hand movement control areas can be clearly noticed. . . . .	68
7-2	Models of the brain (white), the ventricles (blue), and the fMRI activation areas (yellow) extracted from the pre-operative scan after matching it to an intra-operative image acquired after some degree of resection. The bottom picture also displays a slice of the intra-operative SPGR scan. . . . .	70

7-3	2D axial view of pre- and intra-operative grayscale MR images overlaid such that the pre-operative is shown with a threshold (yellow-green) in order to visualize the direction of the brain shift. Red arrows show that the central sulcus has shifted anteriorly by a few millimeters. . .	72
7-4	Models of the brain (blue), the tumor resection cavity (white), pre-operative fMRI activation areas (red), and the fMRI activation areas extracted from the pre-operative scan after matching it to an intra-operative image acquired after some degree of resection (yellow). . . .	73
B-1	Cluster of Sun Microsystems computers. . . . .	80
B-2	Sun Microsystems workstation (Ultra 80). . . . .	81
B-3	Sun Microsystems SMP machine (Enterprise 5000). . . . .	81
B-4	Sun Microsystems file server. . . . .	82

# List of Tables

A.1 Glossary of Abbreviations. . . . .	78
--	----

# Chapter 1

## Introduction

### 1.1 Context of the work

Medical image processing and analysis have evolved very quickly during the past decade and have been raising new challenges for scientists and engineers. The primary importance of medical imaging is that it provides information about the volume beneath the surface of objects. Indeed, images are obtained for medical purposes to probe the otherwise invisible anatomy below the skin. This information may be in the form of the two-dimensional projections acquired by traditional radiography, the two-dimensional slices of ultrasound, single and biplane fluoroscopy (including Digital Subtraction Angiography (DSA)), or full three-dimensional (3D) acquisitions, such as those provided by Computed Tomography (CT), Magnetic Resonance Imaging (MRI), Single Photon Emission Computed Tomography (SPECT), Positron Emission Tomography (PET), functional MRI (fMRI), Magnetic Resonance Angiography (MRA), CT Angiography (CTA), Diffusion Tensor MRI (DTMRI) or 3D Ultrasound (US) [37].

In medical imaging applications, it is often necessary to estimate, track, or characterize complex shapes and motions of internal organs such as the brain or the heart. In such applications, deformable physics-based modeling (which associates geometry, dynamics and material properties in order to model physical objects and their interactions with the physical world) provides the appropriate mechanism for modeling

tissue properties, estimating, characterizing and visualizing the motion of these organs, and for extracting model parameters which can be useful for diagnosis, surgical planning, and surgical guidance [10].

The goal of this thesis was to use a physics-based biomechanical model, designed and developed by Ferrant [10], to capture changes in the brain shape during Image Guided Neurosurgery (IGNS). Such deformations were then applied to critical structures extracted from pre-operatively acquired data of different modalities, in order to make the information provided by such data available to the surgeon during the procedure. We have used High-Performance Computing (HPC) to meet the real-time constraints of neurosurgery, and this allowed for the visualization of multi-modality data, otherwise not available during surgery, together with intra-operative MR data. In the remainder of this chapter, the specific use of medical images during neurosurgery (Section 1.2), the need for image fusion (Section 1.3) and for non-rigid registration (Section 1.4) during IGNS will be described.

## 1.2 Image Guided Neurosurgery (IGNS)

The development of image guided surgery methods over the past decade has permitted major advances in minimally invasive therapy delivery. These techniques, carried out in operating rooms equipped with special purpose imaging devices, allow surgeons to look at updated images acquired during the procedure. This has been particularly helpful for neurosurgical procedures, where the surgeon is faced with the challenge of removing as much tumor as possible without destroying healthy brain tissue. Difficulties here are caused by the similar visual appearance of healthy and diseased brain tissue. This is not always the case, but for many lesions, like low-grade gliomas, it is very difficult for the surgeon to visualize the lesion margins. Also, it is impossible for the surgeon to see critical structures underneath the brain surface as it is being cut. Some vital anatomical information, such as the orientation and the location of dense white matter fiber bundles, may not be visible at all.

Images acquired intra-operatively can provide improved contrast between tissues,

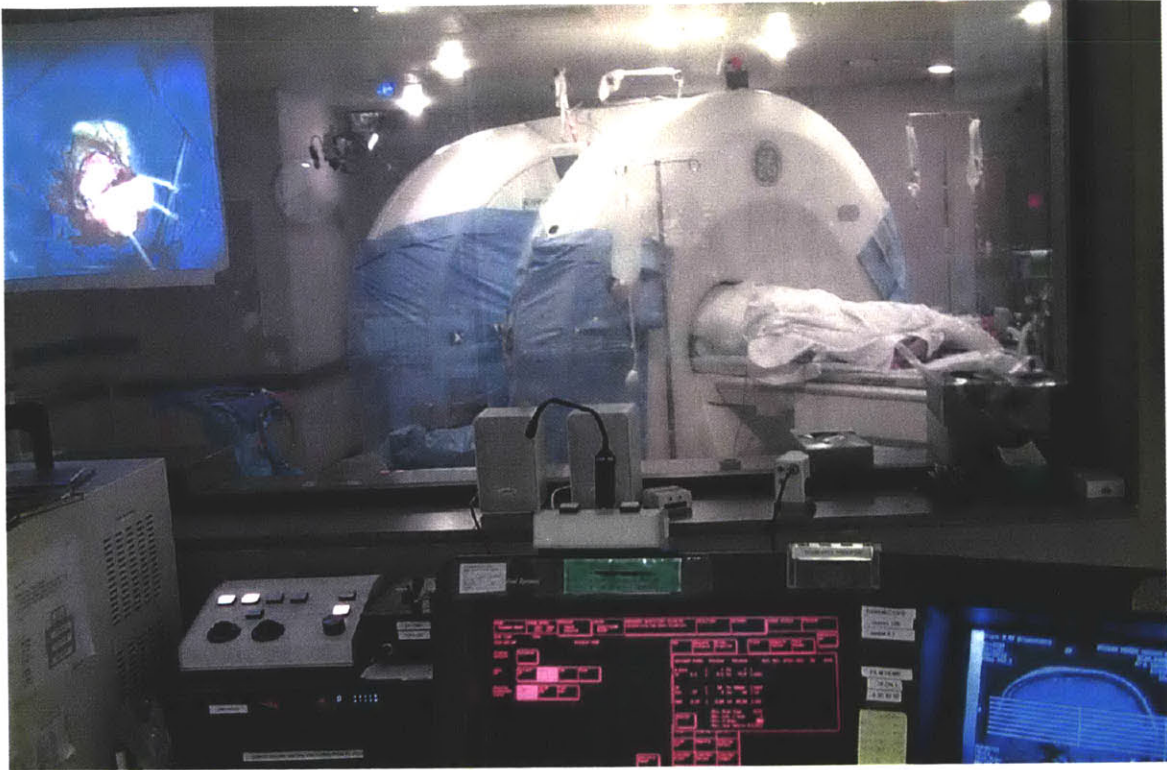


Figure 1-1: Open Magnet MR configuration in the MRT room at the BWH.

and enable seeing past the surface in order to give the surgeon a better appreciation of the deeper structures of the brain. A number of imaging modalities have been used for image guidance; MRI has an important advantage over other modalities due to its high spatial resolution and superior soft tissue contrast, which has proven to be particularly useful for IGNS [4]. Figure 1-1 shows the open magnet MR configuration in the Magnetic Resonance Therapy (MRT) operating room at the Brigham and Women's Hospital (BWH). The MRT room is used to carry out particularly challenging neurosurgical procedures. The surgeon can operate on the patient while he/she is being scanned by the MR system (Signa SP, 0.5 Tesla, General Electric Medical Systems, Milwaukee, WI), which is used to acquire images as necessitated by the procedure.

IGNS has largely been a visualization driven task. In the past, quantitative assessment of intra-operative imaging data has not been feasible, but qualitative judgments by clinical experts have been relied upon. Thus, effort was primarily focused on image



acquisition, visualization and registration of intra-operative and pre-operative data, to provide surgeons with a rich environment from which to derive such judgments. Early work has established the importance of image guidance, which can provide better localization of lesions, the improved localization of tumor margins, and the optimization of the surgical approach [20]. Algorithms for computer-aided IGNS have been developed to improve image acquisition quality and speed, and to provide more sophisticated and capable intra-operative image processing. This led to significant progress in multi-modality image fusion and registration techniques. However, clinical experience in IGNS in deep brain structures and with large resections has exposed the limitations of existing registration and visualization approaches. This motivates the investigation of improved visualization methods and registration algorithms that can capture the non-rigid deformation the brain undergoes during neurosurgery.

### 1.3 Multi-Modality Image Fusion for IGNS

Due to the time constraints of an operating room, the inaccessibility of different contrast mechanisms and the low magnetic field, intra-operative MRI usually results in images with low signal-to-noise ratio. However, visualization during IGNS can be enhanced by pre-operatively acquired data, whose acquisition is not limited by any time restriction, and that can provide increased spatial resolution and contrast. Thus, pre-operative data is able to provide more morphological and functional information than intra-operative data. Multi-modality registration allows pre-surgical data, including modalities that cannot currently be acquired intra-operatively, such as fMRI, MRA, DTMRI, and nuclear medicine scans, such as PET and SPECT, to be visualized together with intra-operative data.

DTMRI, for instance, provides direct visual information about white matter tracts, while it is difficult if not impossible to manually segment these tracts from conventional MR images. Previous work [22] has shown that it is possible to track anatomical structures, such as the corticospinal tract, even if diffusion tensor data is not available during surgery. This was achieved by aligning a deformable volumetric digital

brain atlas onto brain scans of tumor patients that were acquired intra-operatively, and by estimating spatial correspondence between atlas and patient’s brain. Affine registration and non-rigid registration based on 3D adaptive template matching techniques enabled accurate matching of the corticospinal tract to the patient’s brain retrospectively.

## 1.4 Non-Rigid Registration for IGNS

During neurosurgical procedures, the brain undergoes non-rigid deformations [29]; in other words, the spatial coordinates of brain structures and adjacent lesions may change significantly. The leakage of cerebrospinal fluid after opening the dura, the administration of anaesthetic and osmotic agents, hemorrhage, hyperventilation, and retraction and resection of tissue are all contributing factors to the so-called intra-operative “brain shift”. This makes information given by pre-operatively acquired datasets more difficult to exploit during surgery.

Figure 1-2 shows three images acquired intra-operatively, in which the brain shift is very evident. The left-most image was acquired before any skin incision, the center image was acquired after skin incision, while the right-most image was acquired after some degree of resection. Figure 1-3 shows another case, where the left image was acquired before skin incision, the center image was acquired after skin incision, and the right image was acquired after performing some degree of resection. Upper slices show a region near the lesion; lower slices show that, even away from the lesion, the brain shift is very pronounced.

Several image-based and physics-based matching algorithms are being developed to capture these changes in the brain shape, and to create an integrated visualization of pre-operative data in the configuration of the deformed brain. In this work, a biomechanical model was employed, which ultimately may be expanded to incorporate important material properties of the brain, once these are determined. The approach was to use a Finite Element (FE) discretization, by constructing an unstructured grid representing the geometry of key brain structures in the intra-operative dataset, in

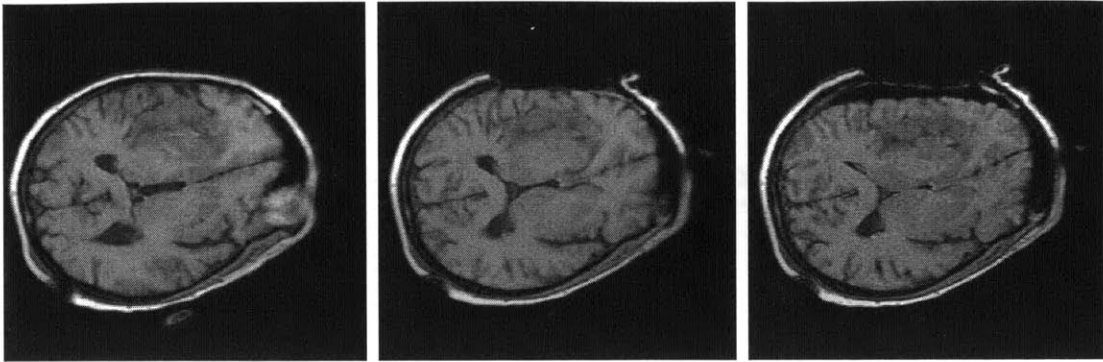


Figure 1-2: Intra-operative MR images. Left: initial image, acquired before skin incision. Center: first intra-operative imaging update, acquired after skin incision. Right: second intra-operative imaging update, acquired after performing some degree of resection.

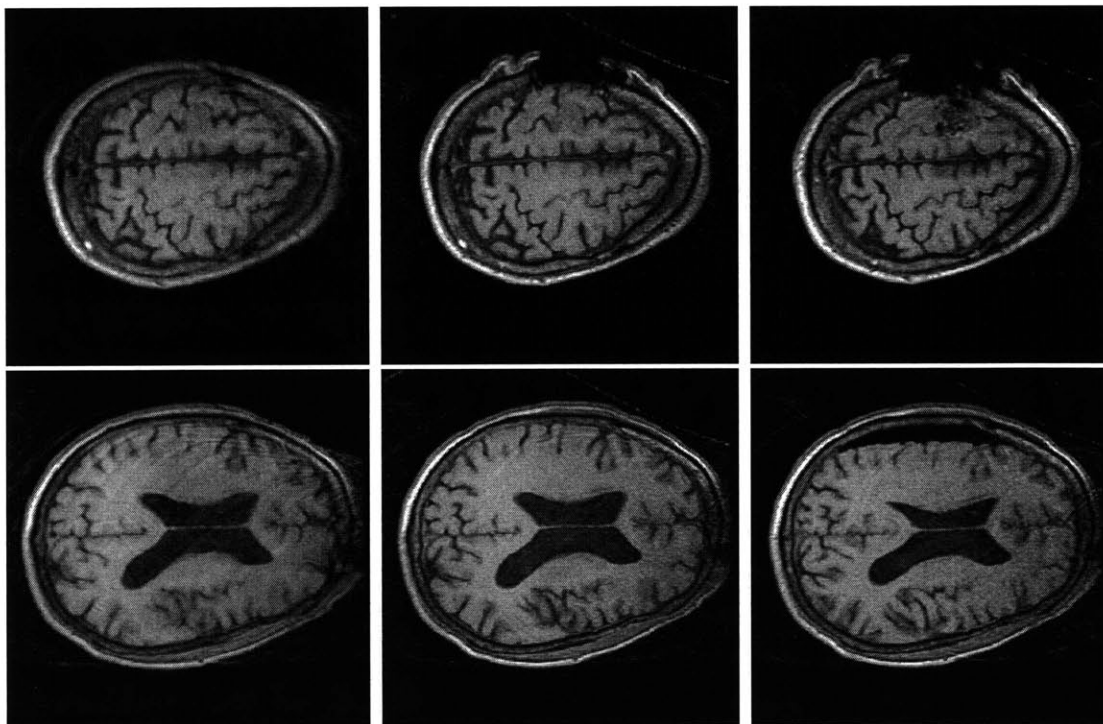


Figure 1-3: Intra-operative MR images. Left: initial image, acquired before skin incision. Center: first intra-operative imaging update, acquired after skin incision. Right: second intra-operative imaging update, acquired after performing some degree of resection. Upper slices show a region near the lesion. Lower slices show that, even away from the lesion, the brain shift is very pronounced.

order to model important regions while reducing the number of equations that need to be solved. The rapid execution times required by neurosurgical operations were achieved by using parallel hardware configurations, along with parallel and efficient algorithm implementations [41].

The deformation of the brain was rapidly and accurately captured during neurosurgery using intra-operative images and a biomechanical registration algorithm developed by Ferrant [10][11][12]. This model has allowed us to align pre-operative data to volumetric scans of the brain acquired intra-operatively, and thus to improve intra-operative navigation by displaying brain changes in three dimensions to the surgeon during the procedure.

## 1.5 Previous Related Work

Methods for tracking the non-rigid deformation taking place within the brain during neurosurgery, in order to visualize pre-operative data matched to intra-operative scans, are in active development. Previous work can be categorized by algorithms that use some form of biomechanical model (recent examples include [16][35][25][13][36]) and algorithms that apply a phenomenological approach relying upon image-related criteria (recent examples include [19][17][18]). Purely image-based matching is expected to achieve a visually pleasing alignment, once issues such as noise and intensity artifact rejection are accounted for. However, in this thesis a physic-based model was favored for intra-operative matching, hence it can ultimately be expanded to incorporate important inhomogenous and anisotropic material characteristics of the brain. An investigation within the domain of physics-based models, ranging from less physically plausible but very fast models to extremely accurate yet requiring hours of compute time biomechanical models, has been carried out.

A fast surgery simulation method, described in [5], was able to achieve high speeds by converting a volumetric FE model into a model with only surface nodes. The aim of this work was to achieve interactive graphics speeds at the cost of the simulation accuracy. Thus, such a model is applicable for computer graphics oriented visualiza-

tions, but not for neurosurgical applications, where robustness and high accuracy are an essential requirement. This thesis describes an accurate matching approach where the clinically compatible execution speeds are achieved via parallel hardware, parallel algorithm design and efficient parallel implementations of these algorithms.

The sophisticated biomechanical model for two-dimensional (2D) simulation of brain deformation using a FE discretization described in [16] used the pixels of the 2D image as the elements of a FE mesh, and relied upon manually determined correspondences. However, during clinical neurosurgical interventions 2D results are not entirely useful. Also, manually determining correspondences is susceptible to operator errors and can be time consuming, especially if a generalization to deal with volumetric anatomy is attempted. In addition, such a discretization approach is particularly computationally expensive (even considering a parallel implementation) if expanded to three spatial dimensions, because of the large number of voxels in a typical intra-operative MRI ( $256 \times 256 \times 60 = 3,932,160$  voxels, implying 11,796,480 displacements to determine), which leads to a large number of equations to solve. Downsampling can provide fewer elements, however it leads to a crude approximation of the true geometry of the underlying anatomy of interest. Instead, the use of a FE model with an unstructured grid (described in Section 3.2) can allow an accurate modeling of key characteristics in important regions of the brain, while reducing the number of equations to be solved by using mesh elements that cover several image pixels in other regions.

Skrinjar et al. [35] described an interesting system for capturing intra-operative brain shift in real-time during epilepsy neurosurgery where the brain shift is rather slow. Brain surface points were tracked to indicate surface displacement, and a simplified homogeneous brain tissue material model was adopted. This model has 2088 nodes, 11733 connections, and 1521 brick elements, and typically required less than 10 minutes on an SGI Octane R10000 workstation with one 250 MHz processor. Following the description of surface-based tracking from intra-operative MR images driving a linearly elastic biomechanical model in [13], a new implementation was presented in [36], which made use of a linear elastic model and surface-based tracking from

intraoperative MRI scans with the goal of eventually using stereoscopic cameras to obtain intra-operative surface data, and thus capture the brain shift.

A 2D three component model with the goal of tracking intra-operative deformation was presented in [9]. In this work, a simplified material model was employed aiming at achieving high speeds. The initial multi-grid implementation on 2D images of 128x128 pixels converged to a solution in 2-3 hours when run on a Sun Microsystems Sparc 20. This is obviously too slow to be practical in clinical neurosurgical practice.

Paulsen et al. [31] and Miga et al. [25][26] have developed a sophisticated FE model to simulate brain deformation, including simulations of forces associated with tumor tissues, and simulations of retraction and resection forces. A clinical application of these models will be very interesting once intra-operative measurements of surgical instrument and associated forces (for instance, the pressure applied by the surgeon with the retractor) is possible. A potential limitation of this approach is that the pre-operative segmentation and the tetrahedral FE mesh generation currently take 5 hours of operator time.

Most meshing software packages used in the medical domain (see [33][14]) do not allow meshing of multiple objects and often work best with regular and convex objects, which is usually not the case for anatomical structures. Therefore, for the purpose of this thesis a tetrahedral mesh generator specifically suited for labeled 3D medical images has been employed. This mesh generator, fully described in [13], can be seen as the volumetric counterpart of a marching tetrahedra surface generation algorithm.

For prediction of brain deformation (rather than capture of brain deformation from intra-operative MR images), more sophisticated models of brain material properties would be required. Miller et al. [27][28] have carried out pioneering simulations and comparison with *in-vivo* data. This study showed that a hyper-viscoelastic constitutive model can reliably predict *in-vivo* brain deformation induced by a force applied with constant loading velocity. This work has great potential for future research in cases when intra-operative images are not available.

Together with physics-based models, mutual information based techniques have

been developed for the purpose of non-rigid registration of medical images. A recent example [32] presents the application of an intensity-based non-rigid registration algorithm with an incompressibility constraint based on the Jacobian determinant of the deformation. This approach provides high-quality deformations while preserving the volume of contrast-enhanced structures. However, in order for such algorithm to be useful in neurosurgical practice, noise and intensity artifacts are issues that still need to be completely solved.

## 1.6 Organization of Thesis Document

This work presents a method for tracking non-rigid brain deformations during IGNS procedures. The first part of the thesis (Chapters 2 to 4) elaborates a step-by-step description of the intra-operative methodology used during several neurosurgical cases. The second part (Chapters 5 to 7) presents results obtained using generic and patient-specific atlases for mapping critical structures during IGNS. The last part of this document (Chapter 8) provides an in-depth discussion of the results and describes directions for future research related to this work.

**Chapter 2** gives an overview of the methodology, and describes the methods used for the segmentation of intra-operative images and for the rigid registration of pre- to intra-operative data.

**Chapter 3** describes the FE based biomechanical model of brain deformation used for non-rigid registration of intra-operative images.

**Chapter 4** describes the visualization environment available in the MRT operating room.

**Chapter 5** shows results obtained by matching a generic deformable volumetric brain atlas during IGNS procedures.

**Chapter 6** shows results obtained by matching patient-specific MRA data to intra-operatively acquired MR images.

**Chapter 7** shows results obtained by matching patient-specific fMRI data to intra-operatively acquired MR images.

**Chapter 8** presents a discussion of the results described in this thesis. In addition, this chapter draws conclusions and provides directions for future research related to this work.



## Chapter 2

# Intra-Operative Methodology: Segmentation and Rigid Registration

This chapter first gives an overview of the methodology used for tracking volumetric brain deformations during IGNS, then it describes two different approaches that have been taken in order to segment intra-operative image data and rigidly register pre- to intra-operative images. This rigid registration is needed because the physics-based deformable registration is more accurate if the images have been previously aligned.

The first approach consists of obtaining a segmentation of the intra-operative scan first, and then using a fast affine registration algorithm to register pre- to intra-operative masked brain segmentations. The second approach consists of rigidly registering pre- to intra-operative grayscale data first, then obtaining a segmentation of the intra-operative data based on that of the pre-operative by means of a tissue classifier.

### 2.1 Methodology Overview

The steps, both pre- and intra-procedural, of the method used for this thesis, can be summarized as follows:

1. **Pre-operative image acquisition and processing:** segmentation and planning of surgical trajectory.
2. **Intra-operative image acquisition** (open magnet MR scanner).
3. **Intra-operative segmentation:** the patient scan is segmented either through an automated multi-channel tissue classifier [44] or through a binary curvature driven evolution algorithm [48]. When this approach is employed, the region identified as brain eventually needs to be interactively corrected to remove any portion of misclassified skin and muscle [15]. Next, this is repeated to obtain a segmentation of the lateral ventricles of the subject.
4. **Intra-operative rigid/affine registration:** the pre-surgical data is registered to the intra-operative patient scan by means of a parallel implementation of an affine registration algorithm [43].
5. **Intra-operative non-rigid registration:** active surface matching and a biomechanical model for volumetric deformation are used to calculate the deformation field and to apply it to the data acquired pre-operatively (see Chapter 3).
6. **Intra-operative visualization:** the matched data is visualized using an integrated system that allows for the display of intra-operative images with pre-operative data together with surface models of key brain structures [15] (see Chapter 4).

Once the next set of scans is obtained and segmented, a new deformation field is calculated and applied to the previously matched data. In this manner, successive images are matched during the procedure. A rigid registration of the intra-operative scans is repeated in the event of patient movement. The flowchart presented in Figure 2-1 shows the intra-operative part of the methodology (items 2-6), which has been the focus of this thesis work.

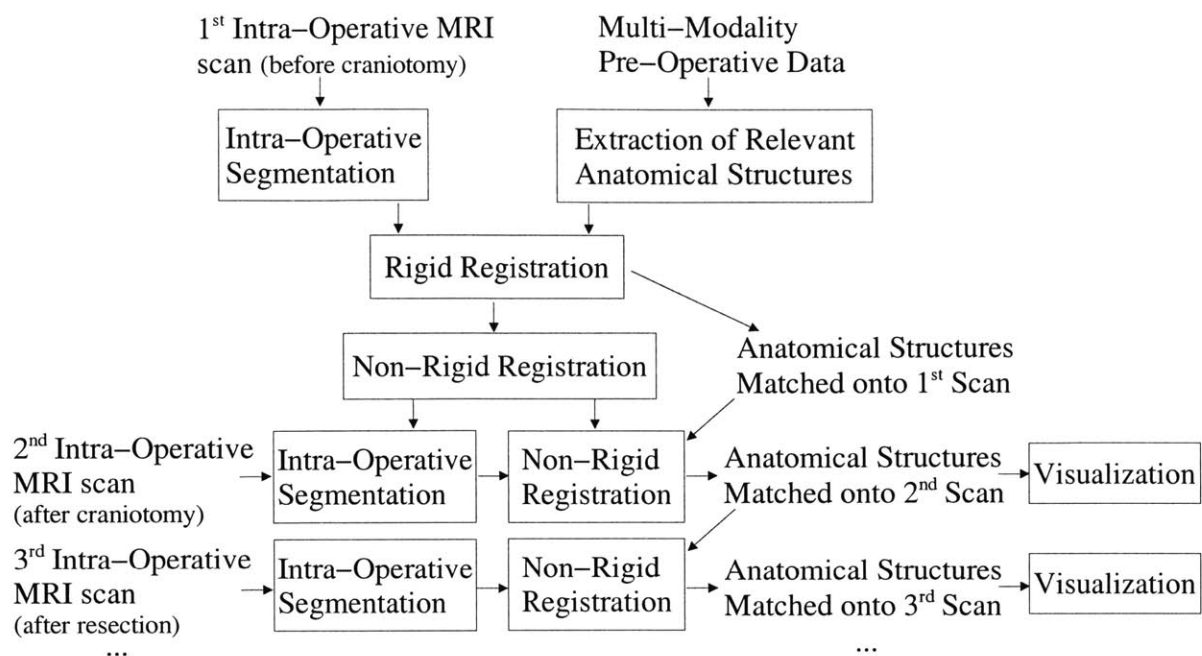


Figure 2-1: Schema for intra-operative segmentation and registration.

### 2.1.1 Pre-Operative Imaging

Before surgery, an MRI examination is performed using a 1.5-Tesla clinical scanner (Signa Horizon; GE Medical Systems, Milwaukee, WI). The standard protocol at the BWH for IGNS cases (the so-called *Protocol 55*) includes the acquisition of the following:

- A T1-weighted, spoiled gradient echo (SPGR) volume (124 1.5mm thick sagittal slices, TR=35msec, TE=5msec, Flip Angle=45, FOV=24cm, matrix=256×192, NEX=1),
- A T2-weighted fast spin echo (FSE) volume (124 sagittal slices, TR=600msec, TE=19msec, FOV=22cm, matrix=256×192, NEX=1),
- A phase-contrast MR angiogram (PC-MRA, 60 sagittal slices, TR=32msec, Flip angle=20, FOV=24cm, matrix=256×128, NEX=1),
- An fMRI exam (HORIZON EPIBOLD sequence, 21 contiguous 7mm coronal slices, TE=50msec, TR=3sec, FOV=24cm, matrix=64×64, 6 alternating 30-

seconds epochs of stimulus and control tasks), given to patients whose pathology is located within the vicinity of the motor cortex.

### **2.1.2 Intra-Operative Imaging**

MRI scans are acquired intra-operatively through an open-configuration MR system (Signa SP; GE Medical Systems, Milwaukee, WI), shown in Figure 1-1. These images are collected 3 to 5 times throughout the duration of every craniotomy, as necessitated by the procedure. These volumes are 3D SPGR (60 2.5mm thick axial slices, TR=28.6msec, TE=12.8msec, FOV=24, matrix=256×128, NEX=1), with imaging times of about four minutes.

## **2.2 Intra-Operative Segmentation and Rigid Registration**

### **2.2.1 Motivation**

The approach described in the next section allows for a very fast segmentation of the intra-operative data. Both brain and lateral ventricles are segmented. The brain segmentation is then used for a fast parallel implementation of an affine registration algorithm. The main motivations for such approach are the speed and the utilization of affine registration, which allows for scaling, in addition to rotation and translation.

### **2.2.2 Segmentation of Intra-Operative Images**

After the acquisition of an intra-operative image, the patient scan is segmented during the neurosurgical procedure either through an automated multi-channel tissue classifier [44] or through a binary curvature driven evolution algorithm [48]. The latter approach (the Riemannian surface evolver, as described by Yezzi et al. in [48]) is the fastest, as it takes only a few seconds to select a threshold and to click inside a region of the brain (or the ventricles). However, it is not as robust as the first approach,

which is a little slower (the tissue classifier is later described in Section 2.3.3). Then, the region identified as brain eventually needs to be interactively corrected to remove any portion of misclassified skin and muscle, using the software described by Gering et al. [15] (this may take a few more minutes).

This procedure is repeated to obtain a segmentation of the lateral ventricles of the subject. Such method allows the neurosurgeon to inspect the segmentations as they are constructed during the surgery and enhances the surgeon’s confidence in their quality.

### **2.2.3 Affine Registration of Pre- to Intra-Operative Images**

After the segmentation of the brain is obtained, this data is masked and used to obtain an affine transformation of the pre-surgical data, so that it is aligned to the intra-operative image. The software used for such alignment is a fast (about 40 seconds) parallel implementation of an affine registration algorithm (minimization of binary entropy) developed by Warfield [43]. This algorithm measures alignment by comparison of dense feature sets (tissue labels) and optimum alignment is found by minimizing the mismatch of the segmentations. The alignment generated minimizes the binary entropy of the aligned data. The parallel implementation distributes resampling and comparison operations across a cluster of symmetric multiprocessors, where the work is load balanced with communication implemented by MPI (Message Passing Interface). This allows the achievement of execution times within a clinically compatible range.

In addition to translation and rotation, accounted for by rigid registration methods, affine registration algorithms also allow for scaling and shearing in images. Since our first tests were conducted with generic atlas data, as a surrogate for pre-operative images, and the head sizes were slightly different, scaling was very important. However, if patient’s pre-operative data is available, the scaling factor can be discarded and a rigid registration algorithm can be used instead, as explained in Section 2.3.

## 2.2.4 Discussion

While the approach described above is very fast, it is not optimal for surgical applications. In order to use the affine registration algorithm, a previous segmentation of the brain is needed. It is desirable, though, to perform the registration first. The segmentation of the intra-operative image, if previously registered to the pre-operative image, becomes then an easier problem. However, the alignment of a statistical atlas of material characteristics, to improve biomechanical modeling, or of a prior model for tissue distribution, to aid in segmentation, would still require an affine registration.

## 2.3 Intra-Operative Segmentation and Rigid Registration: an Alternative Approach

### 2.3.1 Motivation

The affine registration method is a very fast algorithm to register pre- to intra-operative images. However, a previous segmentation of the intercranial cavity is required to achieve high speeds. Thus, we have successfully experimented with a different approach (not shown in the flowchart), which does not require a previous segmentation of the data for registering the images. Such approach is more robust and more appropriate for surgical applications.

### 2.3.2 Rigid Registration of Pre- to Intra-Operative Images

During surgery, the pre-surgical data is aligned with the intra-operative grayscale data using a Mutual Information (MI) based rigid registration method developed by Wells and Viola [46]. This technique attempts to find the registration by maximizing the information that one volumetric image provides about the other. MI is defined in terms of entropy, which is estimated by approximating the underlying probability density. The entropy approximation is then used to evaluate the MI between the two volumes. Finally, a local maximum of MI is found by using a stochastic analog of

gradient descent.

A detailed description of this method can be found in [46]. This approach is slower (a few minutes) than the affine registration approach, but it is more robust and it can be further optimized to obtain the high speeds required by neurosurgical procedures.

### 2.3.3 Segmentation of Intra-Operative Images

Once rigidly registered to the pre-surgical data, the intra-operative data is segmented by means of a tissue classifier as described in [44]. Intra-operative segmentation provides quantitative monitoring of the progress of therapy (allowing for a quantitative comparison with a pre-operatively determined treatment plan), enables the identification of structures not present in previous images, such as surgical probes and changes due to resection, and provides intra-operative surface rendering for rapid 3D interactive visualization.

The image segmentation algorithm we employed takes advantage of an existing pre-operative MR acquisition and segmentation to generate a patient-specific anatomical model for the segmentation of intra-operative data. As the time available for segmentation is longer, images acquired before surgery are segmented through the most robust and accurate approach available for a given clinical application. Each segmented tissue class is then converted into an explicit 3D volumetric spatially varying model of the location of that tissue class, by computing a saturated distance transform of the tissue class [44].

During surgery, the intra-operative data together with the spatial localization model forms a multichannel 3D data set. A statistical model for the probability distribution of tissue classes in the intensity and anatomical localization feature space is also built, then the multichannel dataset is segmented with a spatially varying classification.

### 2.3.4 Discussion

The only drawback of this alternative approach is that it is slower than the first one. However, as mentioned above, the MI based rigid registration algorithm can be tuned to achieve higher speeds in the future. In conclusion, this is the best approach for IGNS applications as both the rigid registration and the tissue classifier are very robust. Also, as we will always use patient's data (the atlas was only used as a first test, to prove that the method was fast enough for surgical applications), an affine registration will not be needed, and the first approach is not suitable.



# Chapter 3

## Intra-Operative Methodology: Non-Rigid Registration

A physics-based biomechanical simulation of brain deformation [12][11][13] was employed to non-rigidly register pre- to intra-operative data. This can be summarized as a four-step process (all the required steps are depicted in the flowchart shown in Figure 3-1).

1. An unstructured surface mesh was generated, where an explicit representation of the surface of the brain and lateral ventricles was extracted based on the pre-operative segmentation. Also, a volumetric unstructured mesh was created using a multiresolution version of the marching tetrahedra algorithm (see Section 3.2).
2. The surfaces of the brain and of the ventricles were iteratively deformed using a dual active surface algorithm (see Section 3.3).
3. The displacements obtained by the surface matching were applied to the volumetric model generated in Step 1. The brain was treated as a homogeneous linearly elastic material (see Section 3.4).
4. Finally, the volumetric deformation fields were applied to the pre-surgical data, from which critical structures were extracted to be displayed to the surgeon (see

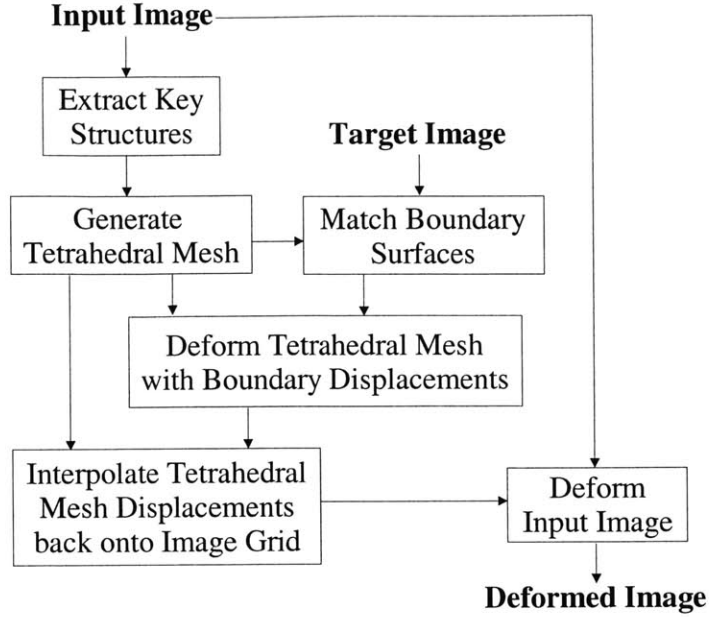


Figure 3-1: Schema of the deformable registration algorithm illustrating the matching of an input image onto a target image.

Section 3.5).

The detailed implementation of Step 1 to Step 3 is fully described in [10]. As the solution of the volumetric biomechanical model requires a great amount of computing resources, a parallel implementation of this algorithm, described in section 3.6, was employed to carry out the non-rigid registration during surgery.

### 3.1 Finite Element Modeling of Elastic Membranes and Volumes

Assuming a linear elastic continuum with no initial stresses or strains, the deformation energy of an elastic body submitted to externally applied forces can be expressed as [49]:

$$E = \frac{1}{2} \int_{\Omega} \sigma^T \epsilon d\Omega + \int_{\Omega} \mathbf{F}^T \mathbf{u} d\Omega \quad , \quad (3.1)$$

where  $\mathbf{u} = \mathbf{u}(\mathbf{x})$  is the displacement vector,  $\mathbf{F} = \mathbf{F}(\mathbf{x})$  the vector representing the forces applied to the elastic body (forces per unit volume, surface forces or forces concentrated at the nodes), and  $\Omega$  the body on which one is working. In the case of linear elasticity, with no initial stresses or strains, the relationship between stress and strain, using a vector notation for  $\sigma$  (stress) and  $\epsilon$  (strain), can be expressed by the generalized Hooke's law as:

$$\sigma = (\sigma_x, \sigma_y, \sigma_z, \tau_{xy}, \tau_{yz}, \tau_{xz})^T = \mathbf{D}\epsilon \quad , \quad (3.2)$$

where  $\mathbf{D}$  is the elasticity matrix characterizing the properties of the material [10] and  $\epsilon$  is the strain tensor (written as a vector for notation simplicity) defined as:

$$\epsilon = (\epsilon_x, \epsilon_y, \epsilon_z, \gamma_{xy}, \gamma_{yz}, \gamma_{xz})^T = \mathbf{L}\mathbf{u} \quad , \quad (3.3)$$

with  $\mathbf{L}$  being the following matrix:

$$\mathbf{L} = \begin{pmatrix} \frac{\partial}{\partial x} & 0 & 0 \\ 0 & \frac{\partial}{\partial y} & 0 \\ 0 & 0 & \frac{\partial}{\partial z} \\ \frac{\partial}{\partial y} & \frac{\partial}{\partial x} & 0 \\ 0 & \frac{\partial}{\partial z} & \frac{\partial}{\partial y} \\ \frac{\partial}{\partial z} & 0 & \frac{\partial}{\partial x} \end{pmatrix} . \quad (3.4)$$

The matrix is symmetric, due to the symmetry of the stress and strain tensors [49]; thus there are 21 elastic constants for a general anisotropic material. In the case of an orthotropic material, the material has three mutually perpendicular planes of elastic symmetry [40]. Hence there are three kinds of material parameters :

- the Young moduli  $E_{ij}$  relate tension and stretch in the main orthogonal directions,
- the shear moduli  $G_{ij}$  relate tension and stretch in other directions than those

of the planes of elastic symmetry,

- the Poisson ratios  $\nu_{ij}$  represent the ratio of the lateral contraction due to longitudinal stress in a given plane.

For a material with the maximum symmetry, i.e. an isotropic material, the material properties are the same in every direction. The elasticity matrix of an isotropic material then has the following symmetric form:

$$D = \frac{E(1-\nu)}{(1+\nu)(1-2\nu)} \begin{pmatrix} 1 & \frac{\nu}{(1-\nu)} & \frac{\nu}{(1-\nu)} & 0 & 0 & 0 \\ \cdot & 1 & \frac{\nu}{(1-\nu)} & 0 & 0 & 0 \\ \cdot & \cdot & 1 & 0 & 0 & 0 \\ \cdot & \cdot & \cdot & \frac{1-2\nu}{2(1-\nu)} & 0 & 0 \\ \cdot & \cdot & \cdot & \cdot & \frac{1-2\nu}{2(1-\nu)} & 0 \\ \cdot & \cdot & \cdot & \cdot & \cdot & \frac{1-2\nu}{2(1-\nu)} \end{pmatrix}, \quad (3.5)$$

where Young's modulus and Poisson's ratio are the same in any direction:  $E = E_x = E_y = E_z$ ,  $\sigma = \sigma_{xy} = \sigma_{xz} = \sigma_{yz}$ . There are no independent shear moduli, as the material parameters are the same in every direction. This therefore reduces the total amount of material parameters to be determined to two.

We model our active surfaces, which represent the boundaries of the objects in the image, as elastic membranes, and the surrounding and inner volumes as 3D volumetric elastic bodies. Within a finite element discretization framework, an elastic body is approximated as an assembly of discrete finite elements interconnected at nodal points on the element boundaries [10]. This means that the volumes to be modeled need to be meshed, i.e. divided into elements, as described in Section 3.2. The elements we use are tetrahedra (where the number of nodes per element is 4) for the volumes and triangles (where the number of nodes per element is 3) for the membranes, with linear interpolation of the displacement field.

For the discretization, the finite element method is applied over the volumetric image domain so that the total potential energy can be written as the sum of potential

energies for each element:

$$E(\mathbf{u}) = \sum_{e=1}^{N_{nodes}} E^e(\mathbf{u}^e) \quad . \quad (3.6)$$

The continuous displacement field  $\mathbf{u}$  within element  $e$  of the mesh is defined as a function of the displacement at the element's nodes  $\mathbf{u}_i^e$  weighted by the element's interpolating functions  $N_i^e(\mathbf{x})$ :

$$\mathbf{u}(\mathbf{x})^e = \sum_{i=1}^{N_{nodes}} \mathbf{I} N_i^e(\mathbf{x}) \mathbf{u}_i^e \quad . \quad (3.7)$$

In order to define the displacement field inside each element, the following linear interpolating function of node  $i$  of tetrahedral element  $e$  is used:

$$N_i^e(\mathbf{x}) = \frac{1}{6V^e} (a_i^e + b_i^e x + c_i^e y + d_i^e z) \quad . \quad (3.8)$$

The computation of the volume of the element  $V^e$  and the interpolation coefficients are described in full details in [49].

For every node  $i$  of each element  $e$ , the following matrix is defined:

$$\mathbf{B}_i^e = \mathbf{L}_i N_i^e \quad , \quad (3.9)$$

where  $\mathbf{L}_i$  is the matrix  $\mathbf{L}$  (see Equation 3.4) at node  $i$ .

The function (Equation 3.1) to be minimized on each element  $e$  can thus be expressed as:

$$E(\mathbf{u}_1^e, \dots, \mathbf{u}_{N_{nodes}}^e) = \frac{1}{2} \int_{\Omega} \sum_{i=1}^{N_{nodes}} \sum_{j=1}^{N_{nodes}} \mathbf{u}_i^{eT} \mathbf{B}_i^{eT} \mathbf{D} \mathbf{B}_j^e \mathbf{u}_j^e d\Omega + \int_{\Omega} \sum_{i=1}^{N_{nodes}} \mathbf{F} N_i^e \mathbf{u}_i^e d\Omega \quad . \quad (3.10)$$

Once the minimum of this function is found at  $\frac{\partial E}{\partial u} = 0$ , Equation 3.10 becomes:

$$\int_{\Omega} \sum_{j=1}^{N_{nodes}} \mathbf{B}_i^{eT} \mathbf{D} \mathbf{B}_j^e \mathbf{u}_j^e d\Omega = - \int_{\Omega} \mathbf{F} N_i^e d\Omega; \quad i = 1, \dots, N_{nodes} \quad . \quad (3.11)$$

This last expression can be written as a matrix system for each finite element:

$$\mathbf{K}^e \mathbf{u}^e = -\mathbf{F}^e \quad , \quad (3.12)$$

where  $\mathbf{K}^e$  and  $\mathbf{F}^e$  are defined as:

$$\begin{aligned} \mathbf{K}_{i,j}^e &= \int_{\Omega} \mathbf{B}_i^{eT} \mathbf{D} \mathbf{B}_j^e d\Omega \\ \mathbf{F}_i^e &= \int_{\Omega} \mathbf{F} N_i^e d\Omega \quad . \end{aligned} \quad (3.13)$$

The coefficients  $i,j$  of the local matrices (corresponding to a pair of  $i,j$  nodes within the local element) are summed up at the locations  $g(i)$   $g(j)$  in the global matrix (where  $g(i)$  represents the number of the element's node in the entire mesh). The assembly of the local matrices into large matrices characterizing the entire simulation then leads to the global system:

$$\mathbf{K} \mathbf{u} = -\mathbf{F} \quad . \quad (3.14)$$

The solution to this system will provide the deformation field corresponding to the global minimum of the total deformation energy.

These are constitutive equations that model surfaces as elastic membranes and volumes as elastic bodies. Given externally applied forces  $\mathbf{F}$  to a discretized body characterized by a rigidity matrix  $\mathbf{K}$ , solving Equation 3.14 provides the resulting displacements, which can then be used to characterize the deformation the brain has undergone during the course of surgery [10].

## 3.2 Mesh Generation

Medical images are represented by an array of a finite number of image samples, or voxels. These could be used as discretizing elements of a FE model; however, to limit computational complexity, it is desirable to work with fewer elements. This implies that many elements will cover several image samples. For computational ease and because they provide better representations of the domains, triangular elements are

chosen to represent surfaces and tetrahedral elements to represent volumes.

A new tetrahedral mesh generator, specifically suited for meshing anatomical structures using 3D labeled images, has been developed by Ferrant [10]. This approach combines the ideas of volume tetrahedralization proposed by Nielson and Sung [30] (iso-voluming) and recursive mesh subdivision (octree subdivision).

An initial multi-resolution, octree-like tetrahedral approximation of the volume to be meshed is computed depending on the underlying image content. Next, an iso-volume tetrahedralization is computed on the initial multi-resolution tetrahedralization, such that it accurately represents the boundary surfaces of the objects depicted in the image [10].

The algorithm first subdivides the image into cubes of a given size, which determine the resolution of the coarsest tetrahedra in the resulting mesh. The cubes are then tetrahedralized, and at locations where the mesh needs better resolution (i.e. smaller edges), the tetrahedra are further divided adaptively into smaller tetrahedra, yielding an octree-like mesh. This subdivision causes cracks for tetrahedra that are adjacent to subdivided tetrahedra. In this case the neighboring tetrahedra are re-meshed using a precomputed case table. The resulting mesh contains pyramids and prisms, which are further tetrahedralized. Finally, the labels of the vertices of each tetrahedron are checked in a marching tetrahedra fashion. If the tetrahedron lies across the boundary of two objects with a different label, it is subdivided along the edges on the image's boundary so as to have an exact representation of the boundary between the objects. The resulting mesh contains prisms, which are further tetrahedralized [10].

### 3.3 Active Surface Deformation

The equations modeling elastic membranes presented in Section 3.1 can be used to solve tracking problems in 3D images by means of deformable surface models. Deformable or active contours were introduced by Kass et al. [21], and have been used increasingly in the fields of computer vision and medical image analysis for seg-

mentation, registration and shape tracking or shape recovery. An active contour is characterized by three parts [10]:

- *internal forces* - elasticity and bending moments describing the contour as a physical object, designed to hold the curve together, and locally smooth (first order terms) as well as keeping it from bending too much (second order terms);
- *external forces* - forces describing how the active contour is attracted to the desired features of the image data;
- *iterative procedure* - process which attempts to find the configuration that best matches both the internal and external forces.

The 2D active contour model has been extended to 3D surfaces by Cohen and Cohen [6], who also proposed to discretize the resolution of the equations governing the behavior of the surfaces using finite elements. In this way, the iterative variation of the surface can be discretized using finite differences, provided the time step  $\tau$  is small enough. Image-derived forces  $\mathbf{F}^{\mathbf{v}^t}$  (forces computed using the surfaces nodal position  $\mathbf{v}$  at iteration  $t$ ) are applied to the active surface to deform it. The constitutive equation for elastic membranes for the active surface (see Equation 3.14) yields to the following iterative equation:

$$\frac{\mathbf{v}^t - \mathbf{v}^{t-1}}{\tau} + \mathbf{K}\mathbf{v}^t = -\mathbf{F}^{\mathbf{v}^{t-1}} \quad , \quad (3.15)$$

which can be rewritten as [10]:

$$(\mathbf{I} + \tau\mathbf{K})\mathbf{v}^t = \mathbf{v}^{t-1} - \tau\mathbf{F}^{\mathbf{v}^{t-1}} \quad . \quad (3.16)$$

The external forces driving the elastic membrane towards the edges of the image structure are integrated over each element of the mesh and distributed over the nodes belonging to the element using its shape functions (see Equation 3.7). The image force  $\mathbf{F}$  is computed as a decreasing function of the gradient such that it is minimized at the edges of the image [21][6]. For correct convergence, the surfaces need to be



initialized very close to the edges of the object to which they need to be matched. Prior information about the surface to be matched (e.g for atlas matching, or in the case of tracking) gives an initial global repositioning of the surface and can be very useful to account for global shape changes such as rescaling and rotation [10]. The distance measure can be efficiently computed by precomputing the distance from any pixel to the reference surface using the Distance Transform algorithm described in [7]. Such a transform provides a good initialization for running an active surface algorithm next that can then account for local shape changes of the surface.

To increase the robustness and the convergence rate of the surface deformation, the forces are computed as a gradient descent on a distance map of the edges in the target image. This distance map is computed using a fast distance transformation algorithm [7]. In addition, the expected gradient sign of the edges is included in the force expression [10]. Thus, the external force can be described by the following expression:

$$\mathbf{F}(\mathbf{x}) = S_{min} G_{exp} \nabla(\mathcal{D}(I(\mathbf{x}))) \quad , \quad (3.17)$$

where  $\mathcal{D}(I(\mathbf{x}))$  represents the distance transformation of the target image at point  $\mathbf{x}$ .  $S_{min}$  is chosen so that the gradient points towards a point with a smaller distance value, while  $G_{exp}$  is the contribution of the expected gradient sign on the labeled image [10].

### 3.4 Biomechanical Volumetric Deformation

Physically realistic models for surgical planning and image registration have recently gained increased attention within the medical imaging community. In fact, purely image-based statistical methods do not take into account the physical properties of the objects depicted in the image and often cannot predict changes in the image, especially when dealing with medical image data. Different objects present in the image have different properties and react in ways defined by their material characteristics (e.g. bone and soft tissue have a very different behavior when submitted to equivalent stresses). Thus, a model developed by Ferrant [10], which incorporates the objects

physical characteristics, has been chosen for the purpose of this thesis, in order to improve the accuracy of the deformable registration.

During IGNS procedures, it can be useful to deform volumes rather than just surfaces, as surfaces are used to represent volumetric objects. Thus, it is possible to deform an initial image onto a target image by imposing regularity constraints, which maintains the spatial relationship between the objects depicted in the initial image. An algorithm for doing elastic image matching using a finite element discretization was developed [10][13][12][11], with the idea of modifying the constitutive equation of volumetric bodies described in Section 3.1 to incorporate the image similarity constraint into the expression of the potential energy of an elastic body submitted to external forces (Equation 3.1). The elastic potential energy then serves as a physics-based regularity constraint to the image similarity term. The full details of the mathematical formulation of the volumetric elastic image matching using the FE method can be found in [[10], Section 5.2].

Thus, the solution of this method for doing physics-based registration of images is to use boundary deformation of the important structures to infer a volumetric deformation field. The algorithm presented in Section 3.3 was used to track the deformation of boundary surfaces of key objects and that deformation was used as input to a volumetric FE elastic model, such as described in Section 3.1. This approach yields a deformation field satisfying the constitutive equations of the body, and can be used to characterize the deformation the body has undergone from the initial to the target image [10].

### **3.5 Application of Volumetric Deformation Fields to Image Data**

Finally, the volumetric deformation fields are applied to image datasets, usually the initial intra-operative image (grayscale or segmentation) and other pre-operative images (such as MRA, fMRI, etc.). Such deformed data can then be visualized using

an integrated visualization system as described in Chapter 4.

Once the next set of scans are obtained and segmented, new meshes are generated, the next set of surfaces are matched, and a new deformation field is calculated and applied to the previously matched data. In this manner, successive scans can be matched during the neurosurgical procedure. The entire method, including segmentation, rigid and deformable registration, is usually completed in less than 12 minutes.

### 3.6 HPC Implementation

The displacements generated by the active surface model are used as boundary conditions, such that the surface displacements of the volumetric mesh are fixed to match them. The volumetric deformation of the brain is then computed by solving for the displacement field that minimizes the energy described by Equation 3.1. Typically, the brain meshes we use have around 25,000 discretization nodes, leading to 75,000 unknown displacements to solve for.

For each element of the finite element mesh, three variables must be determined, which represent the  $x$ ,  $y$  and  $z$  displacements. Each variable corresponds to one row and one column in the global  $\mathbf{K}$  matrix. The rows of the matrix are divided equally among the processors that are available for computation, and the global matrix is assembled in parallel. Each element in the subdomain of the local  $\mathbf{K}^e$  matrix is assembled by each CPU (Central Processing Unit). Following matrix assembly, the boundary conditions determined by the active surface matching algorithm are applied. The global  $\mathbf{K}$  matrix is adjusted such that rows, which are associated with variables that are determined, consist of a single non-zero entry of unit magnitude on the diagonal.

When solving such large systems, the connectivity count of the nodes in the mesh plays an important role: the lower it is, the less elements the matrix will have. In addition, to optimize the parallelization of the assembly and resolution of large systems, the connectivity count needs to be constant throughout the mesh to avoid load

balancing problems: if the nodes managed by a processor have a higher connectivity than those of another processor, this CPU will have to do more computations to perform the system assembly. Therefore, even if each processor has an equal number of rows to process, because of the irregular connectivity of the mesh, some processors may perform more work than others.

The MPI was used to parallelize the assembly of the matrix systems, and to optimize memory allocation of the different processors across the matrix system. Both the active surface membrane model and the volumetric biomechanical brain model system of equations are solved using the Portable, Extensible Toolkit for Scientific Computation (PETSc) package [1][2] using the Generalized Minimal Residual (GMRES) solver with Jacobi preconditioning. During neurosurgical procedures, the system of equations was solved on a Sun Microsystems SunFire 6800 Symmetric Multiprocessor (SMP) system with 12 750MHz UltraSPARC-III (8MB Ecache) CPU's and 12 GB of RAM (more details about the computing resources available at the SPL can be found in Appendix B). This architecture provides sufficient compute capacity to execute the intra-operative image processing prospectively during neurosurgery.

## Chapter 4

# Intra-Operative Methodology: Visualization

The last step of our method for tracking non-rigid changes in the brain anatomy during IGNS involves the visualization of such deformations in the operating room. We chose to use the 3D Slicer [15], an integrated surgical guidance and visualization system which provides capabilities for data analysis and on-line interventional guidance. The 3D Slicer allows for the display of intra-operative images along with pre-surgical data, including surface renderings of previous triangle models and arbitrary interactive resampling of 3D grayscale data. This system also provides the visualization of virtual surgical instruments in the coordinate system of the patient and patient image acquisitions. The images we constructed were presented on the LCD monitor in the MRT operating room, and increased the information available to the surgeon as the operation progressed.

The 3D Slicer is the platform of choice for IGNS procedures in the MRT room. It was developed mainly by Gering and O'Donnell [15] at the SPL. It allows to selectively display the information available in the system, which may be in the form of MR scans, surface models, etc. A screen shot of the system windows is shown in Figure 4-1. More information can be found at <http://www.slicer.org>.

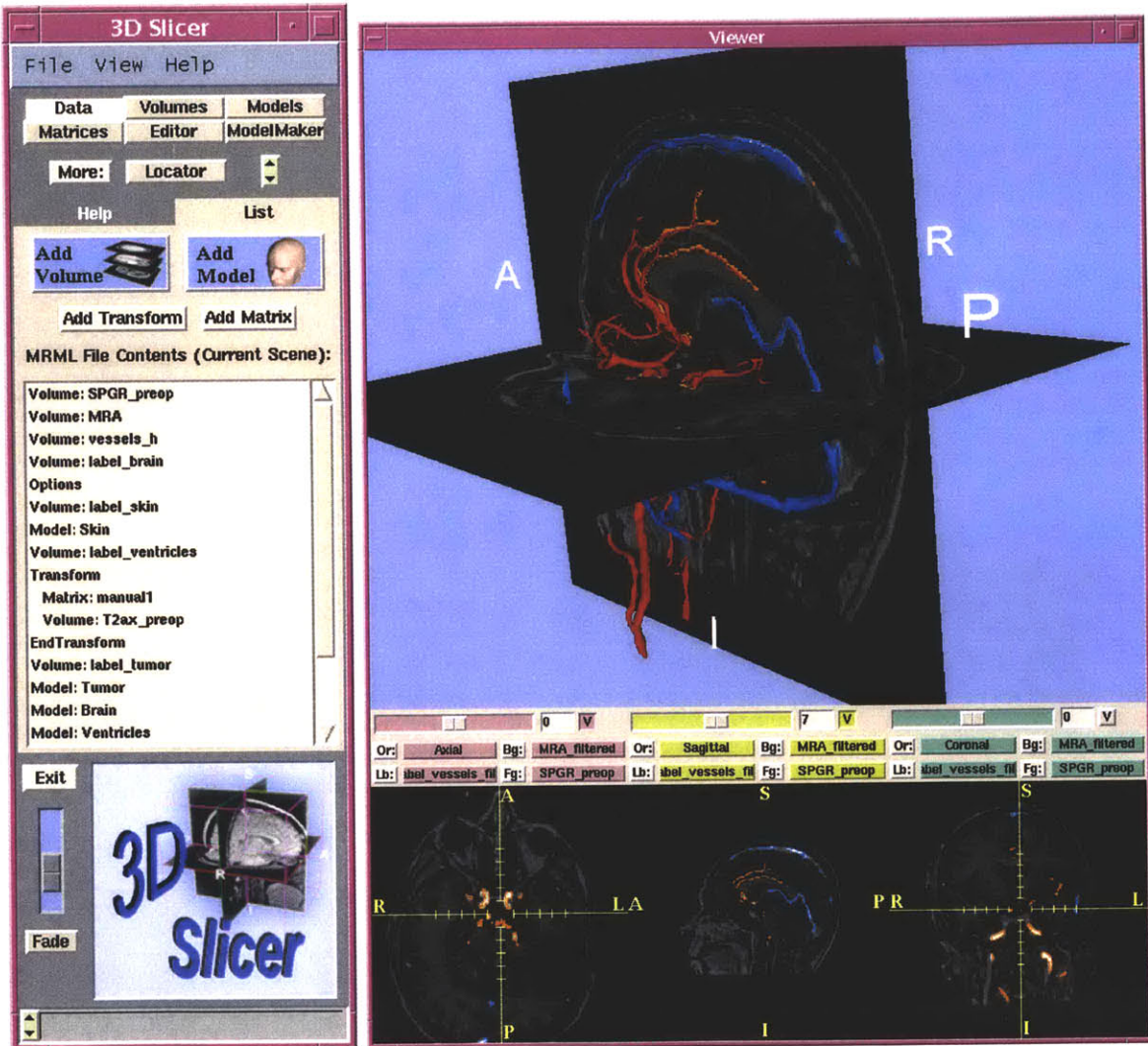


Figure 4-1: Screen shots of the 3D Slicer.

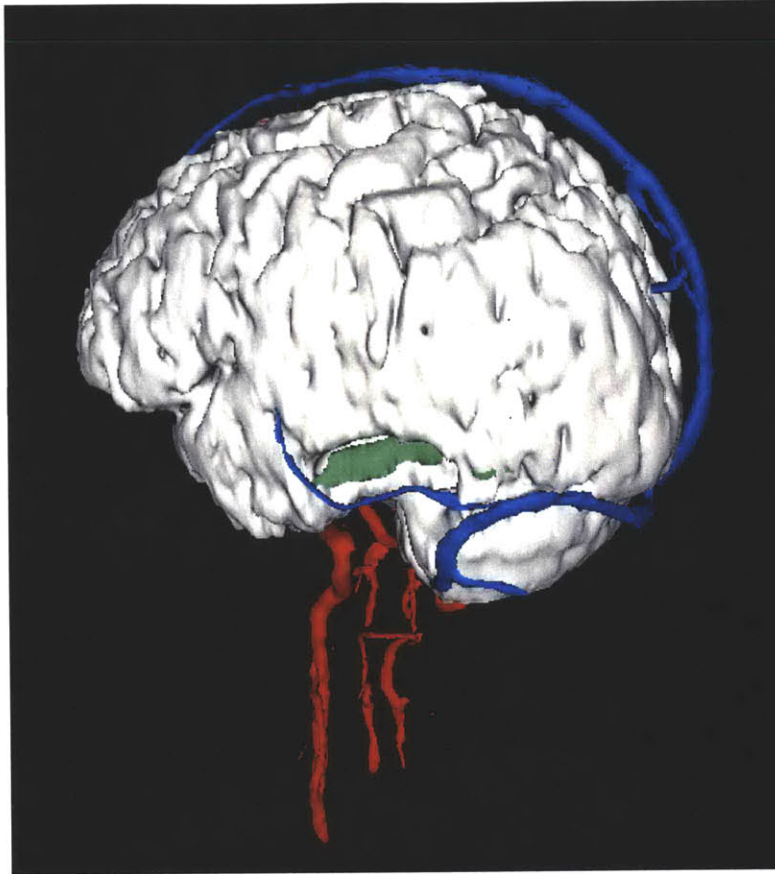


Figure 4-2: Multi-modality image fusion: Surface models of brain (white) and residual tumor (green), generated from an intra-operative image acquired after some degree of resection, are shown together with surface models of arteries (red) and veins (blue), generated from pre-operative MRA data.

## 4.1 Multi-Modality Image Fusion

Intra-operative images provide the neurosurgeon with a great deal of information. However, for difficult surgical procedures, it is beneficial to present the surgeon with not just one diagnostic scan, but with an array of information derived from fusing multi-modality datasets containing information on morphology (MRI, CT, MRA), cortical function (fMRI), and metabolic activity (PET, SPECT). A shortcoming of this approach is that pre-operatively acquired images do not account for changes in brain morphology that occur during the procedure. Applying a non-rigid deformation algorithm, as described in Chapter 3, to the pre-operative data, allows this visualization system to actually provide reliable information during IGNS procedures. Results

of the deformable registration of multi-modality data are shown in Chapters 5 to 7.

Various pre-procedural scans (T1- and T2-weighted MRI, MRA, fMRI) are fused and automatically aligned with the operating field of the interventional MR system by a rigid registration first (see Chapter 2) and a deformable registration after (see Chapter 3). Pre-operative data is segmented in order to generate 3D surface models of key brain structures, such as brain, ventricles, tumor, skin, arteries, veins, etc. Intra-operative data is segmented as well (brain and ventricles are needed for the non-rigid registration algorithm) and models are combined in a three-dimensional scene, as shown in Figure 4-2. The structures displayed in this figure have been rigidly registered (the results of the deformable registration of vessels onto intra-operative data are shown later in Chapter 6).

Reformatted slices of MR images acquired during surgery can be also shown along with the models. Surface models are generated from the segmentations using the marching cubes algorithm and decimation; each model is colored differently and rendered with adjustable opacity [15]. Thus, pre-surgical data, non-rigidly aligned to intra-operative images, augments interventional imaging to expedite tissue characterization and precise localization and targeting.

## 4.2 Intra-Operative Navigation

The scene presented to the surgeon consists not only of models of critical brain structures, as explained in Section 4.1, but also of reformatted slices that are driven by a tracked surgical device. The location of the imaging plane is specified with an optical tracking system (Flashpoint; Image Guided Technologies, Boulder, CO). The spatial relationship (position and orientation) of this system relative to the scanner is reported with an update rate of 10Hz. A visualization workstation (Ultra 30; Sun Microsystems, Mountain View, CA) is connected to the MR scanner with a TCP/IP network connection, and contains two Sun Creator 3D graphics accelerator cards. One drives the 20-inch display in the control area of the surgical suite, and the other outputs the 3D view to color LCD panels inside the scanner gantry.



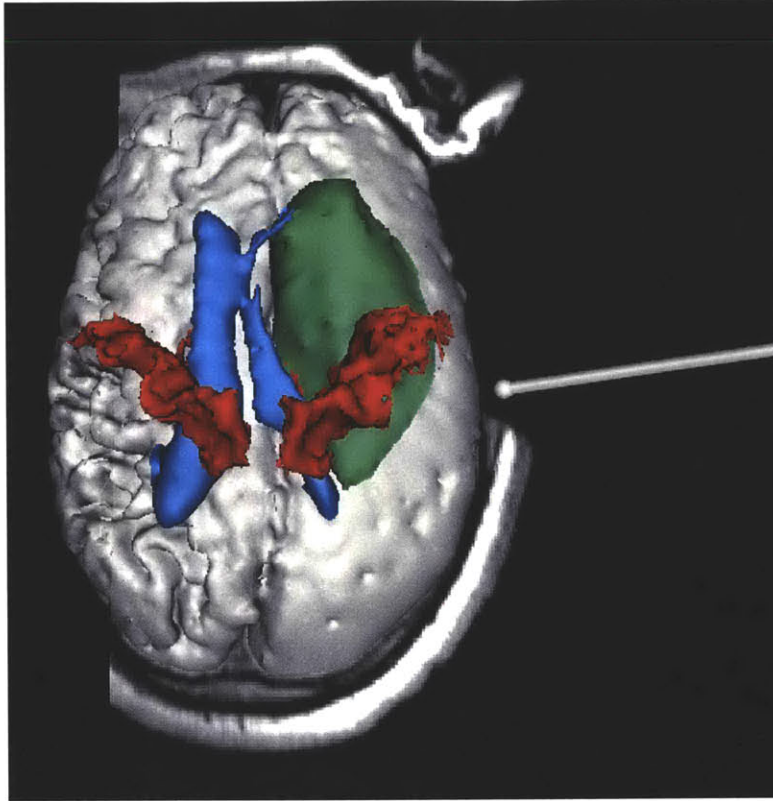


Figure 4-3: Intra-operative navigation: Surface models of the brain (white), the ventricles (blue), the corticospinal tract (red) and the tumor (green), generated from pre-operative and intra-operative data, are displayed aligned with an intra-operative SPGR scan and together with the virtual surgical instrument tracked in the coordinate system of the patient's image acquisition.

Whenever the position and orientation of the optical tracking system change, or a new image is acquired, a server process sends the new data to the 3D Slicer software resident on the visualization workstation. In this way, surface models, generated from pre- and intra-operative data, are visualized together with the tracked surgical instrument as shown in Figure 4-3. In this case, surface models of the brain (white), the ventricles (blue), the corticospinal tract (red) and the tumor (green), generated from pre-operative and intra-operative data, are displayed aligned with an intra-operative SPGR scan and together with the virtual surgical instrument tracked in the coordinate system of the patient's image acquisition.

## Chapter 5

# Deformable Atlas-based Tracking of Critical Brain Structures during IGNS

The work presented in this chapter is also described in [39], which was published in the proceedings of the *VISIM: Information Retrieval and Exploration in Large Medical Image Collections* workshop, held in conjunction with *MICCAI 2001: the Fourth International Conference on Medical Image Computing and Computer Assisted Intervention*, in Utrecht, the Netherlands, on October 14-18, 2001. This work was orally presented at the *VISIM* workshop as well.

### 5.1 Motivation

As an initial test, a deformable volumetric brain atlas, based on MR imaging of a single normal male where each voxel was labeled according to its anatomical membership [23], was used to map brain structures onto images acquired during three neurosurgical procedures. This allowed for the visualization of complex anatomical information that would otherwise require the use of additional modalities during neurosurgery. However, as this is a generic atlas, it has limited clinical value. It was used as a surrogate for patient-specific pre-surgical data, in order to prove that this

method meets the real-time constraints of neurosurgery.

## 5.2 Description

Previous work by Kaus [22] has shown that it is possible to track anatomical structures, such as the corticospinal tract, even in cases when DTMRI data is not available during neurosurgery. Tracking the corticospinal tract can be useful if the tumor is located in its proximity. Such cases are frequent, however it is not an unusual situation that other critical structures are situated near the tumor site, and thus need to be tracked during a neurosurgical procedure. Examples of such structures are parts of the visual system: the optic radiation and the lateral geniculate body. Here we show the application of our method to one case where the tumor was located anterior to the pre-central gyrus, very close to the corticospinal tract, and to another case, where the tumor was located in the posterior left temporal lobe, in close anatomical relationship to the optic radiation.

Our approach uses a finite element model, which simulates brain elastic properties, to infer the deformation fields captured from the intra-operative image updates and to compensate for brain shift during neurosurgery. This algorithm was designed to allow for improved surgical navigation and quantitative monitoring of treatment progress in order to improve the surgical outcome and to decrease the time required in the MRT room. To our knowledge, this represents the first time such an approach has been applied prospectively, rather than retrospectively using images acquired during the surgical procedure for post-processing purposes. High-performance computing is a key enabling technology that allows the biomechanical simulation to be executed quickly enough to be practical in clinical use during neurosurgery.

A deformable volumetric brain atlas was used to track critical brain structures onto intra-operative images acquired during three neurosurgery cases. Images of head muscles and central nervous system structures, which are part of the generic atlas employed for this thesis, are shown in Figure 5-1 [34]. A close look at the visual system is presented in Figure 5-2 [34] at the top. For the purpose of hierarchical registration, a

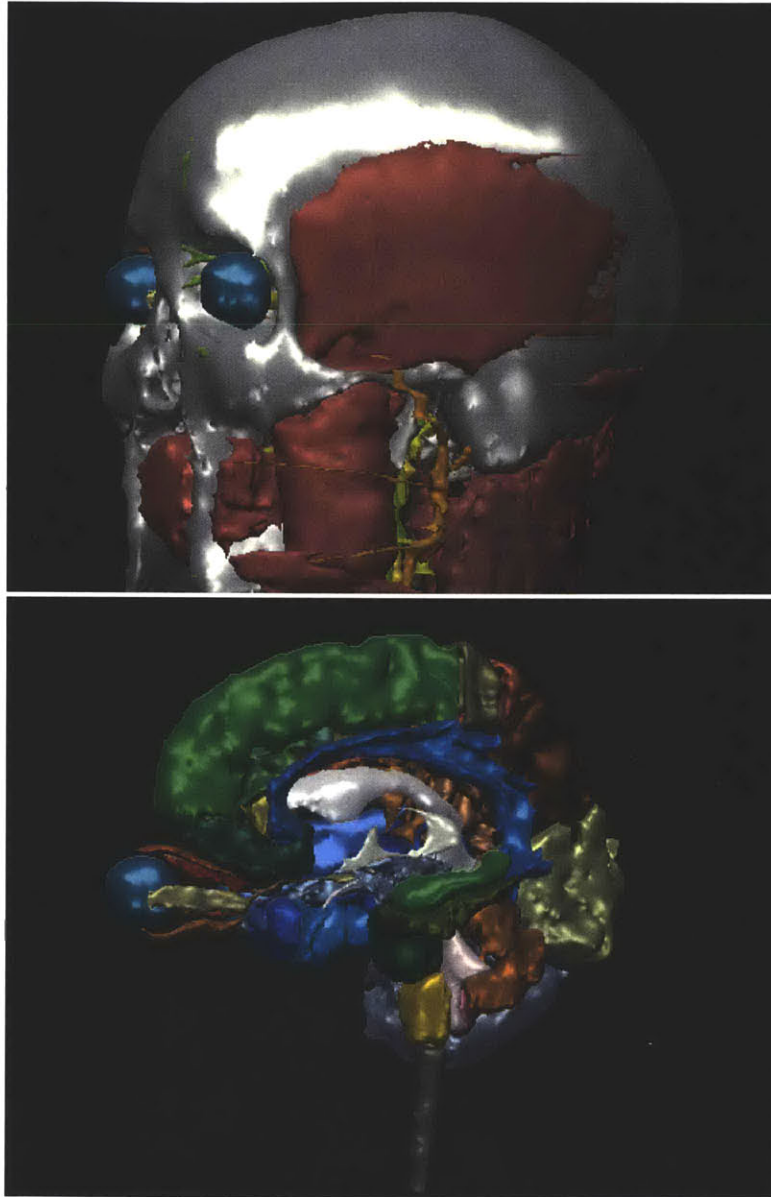


Figure 5-1: Head muscles (top) and central nervous system structures (bottom) of the generic brain atlas used for intra-operative matching.

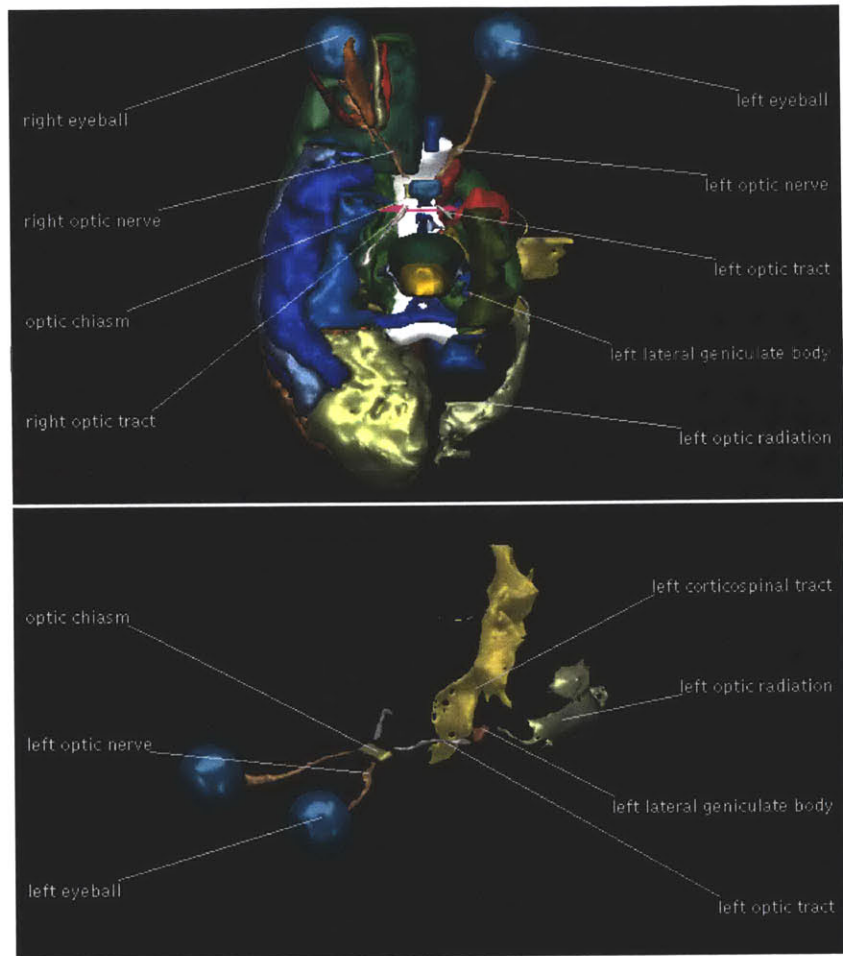


Figure 5-2: Top: Visual system extracted from the generic brain atlas used for intra-operative matching. Bottom: Image of structures such as corticospinal tract and optic radiation, which were needed for neurosurgical cases, and were therefore extracted from the generic atlas.

separate template volume containing only one structure (i.e. the corticospinal tract or the optic radiation) was extracted. Images of such structures are shown at the bottom of Figure 5-2 [34]. The results of the intra-operative match, shown in the next section, were displayed to the neurosurgeon in the operating room. Such visualizations allowed the surgeon to make judgments based on the anatomical information contained in the matched image.

### 5.3 Results

In this section, results of two different cases are presented. In the first case, the optic radiation was tracked during the surgical procedure, as the tumor was located in its proximity. The second case required the matching of the corticospinal tract. Figure 5-3 shows post-resection models of the brain (white), the ventricles (blue), the tumor (green), and the optic radiation (yellow). The tumor is clearly located next to the optic radiation. It is also to be noticed that, after most of the resection, the brain has shifted significantly. While the top images are useful for engineering purposes, they do not contain any “real” data to be eventually referenced. On the other hand, the bottom images show the models along with the intra-operatively acquired MR dataset. Such views are much more valuable to the surgeon, who can still make judgments based on the raw anatomy.

Figure 5-4 shows another view which is very important for surgical practice, and which presents the navigation capabilities of the 3D slicer as well. This picture shows an intra-operative MR dataset acquired during the second case aligned with the corticospinal tract extracted from the deformed atlas, displayed with the virtual surgical needle, interactively tracked within the patient’s coordinate system.

In Figure 5-5 pre- and post-resection models of the brain (white), the ventricles (blue) and the corticospinal tract (pink) are shown respectively on the left and on the right. The top images present only models of the brain, in order to show how significant the brain shift is during a neurosurgical procedure. The bottom images show the same views with all other models, so that it is evident that the tumor was

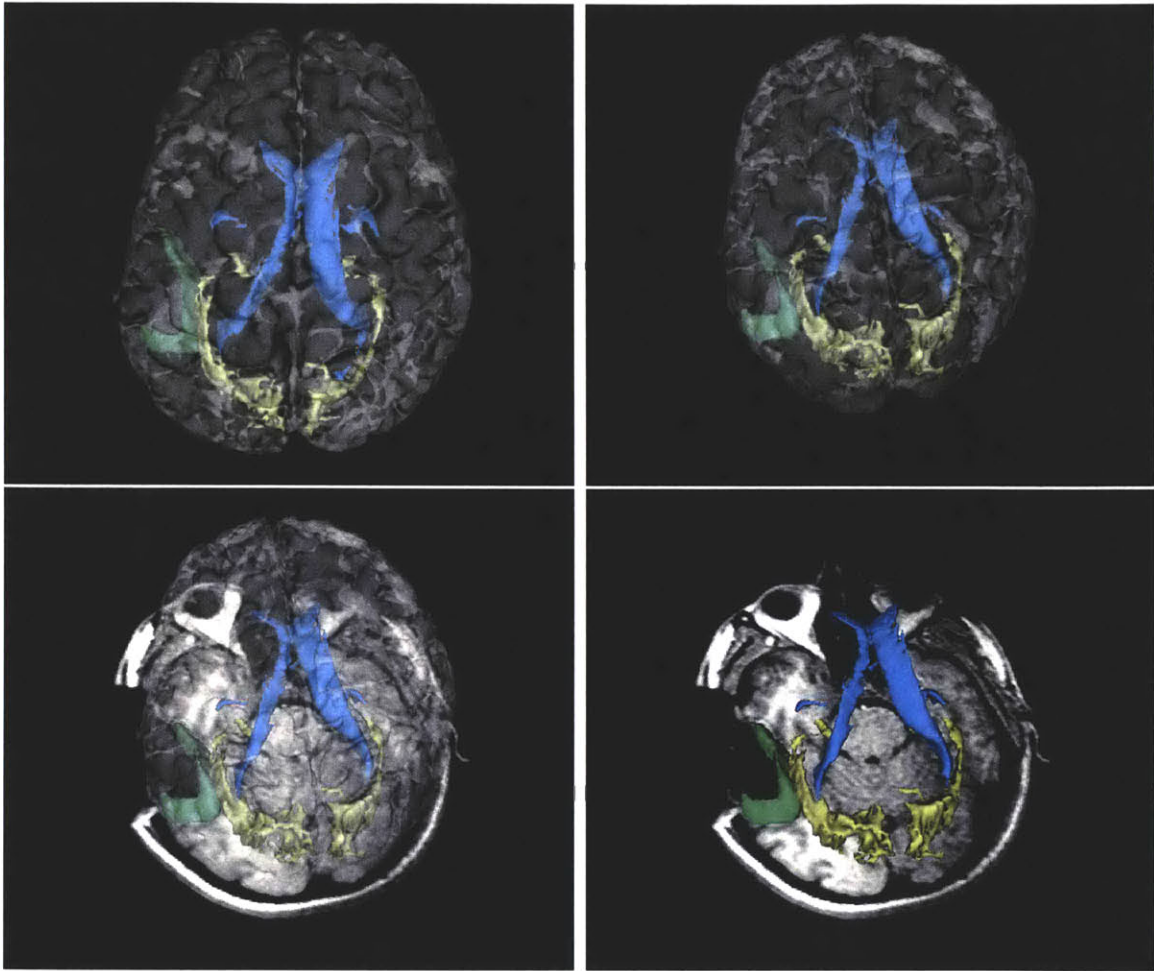


Figure 5-3: Post-resection models of the brain (white), the ventricles (blue), the tumor (green) and the optic radiation (yellow). The tumor is clearly located next to the optic radiation. After most of the resection, the brain has shifted significantly. In the bottom images, the models are shown along with the intra-operatively acquired MR dataset.

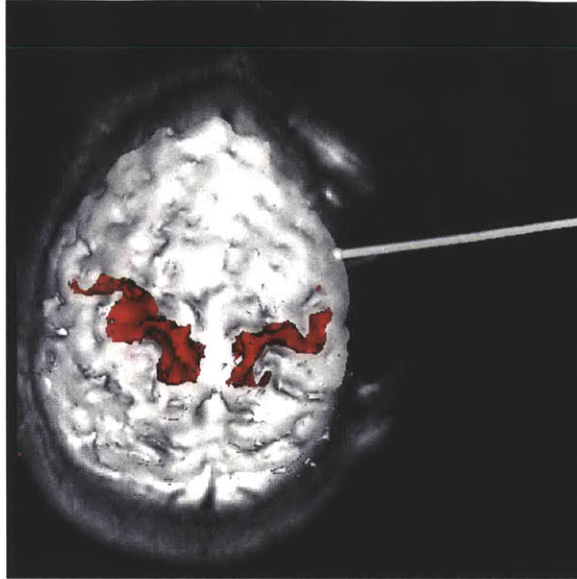


Figure 5-4: Intra-operative MR dataset aligned with the corticospinal tract extracted from the deformed atlas, displayed with the virtual surgical needle, interactively tracked within the patient's coordinate system.

located in close anatomical relationship to the corticospinal tract.

Figure 5-6 presents different visualization of deformation fields that were calculated during the matching of the first intra-operative scan volume onto the second intra-operative scan volume of the second case. The top images show deformation fields on the surface of the brain, while the middle and bottom images show deformation fields across the whole brain volume. In the bottom images, the volumetric deformation fields are shown aligned with the corticospinal tract (blue). The color-coding indicates the magnitude of the deformation at every point on the surface or cuts of the deformed volume, and arrows indicate the magnitude and direction of the deformation.

As shown in the figures, the deformation was accurately calculated and it was possible to register the atlas corticospinal tract or optic radiation to the patient anatomy. A small registration error is present due to the fact that patient's and atlas brain have a very different morphology, as the atlas is not specific to the patient [39]. In these initial experiments, a generic atlas was used as a surrogate for pre-operative data from different imaging modalities (MRA, fMRI, etc.). More rigorous validation



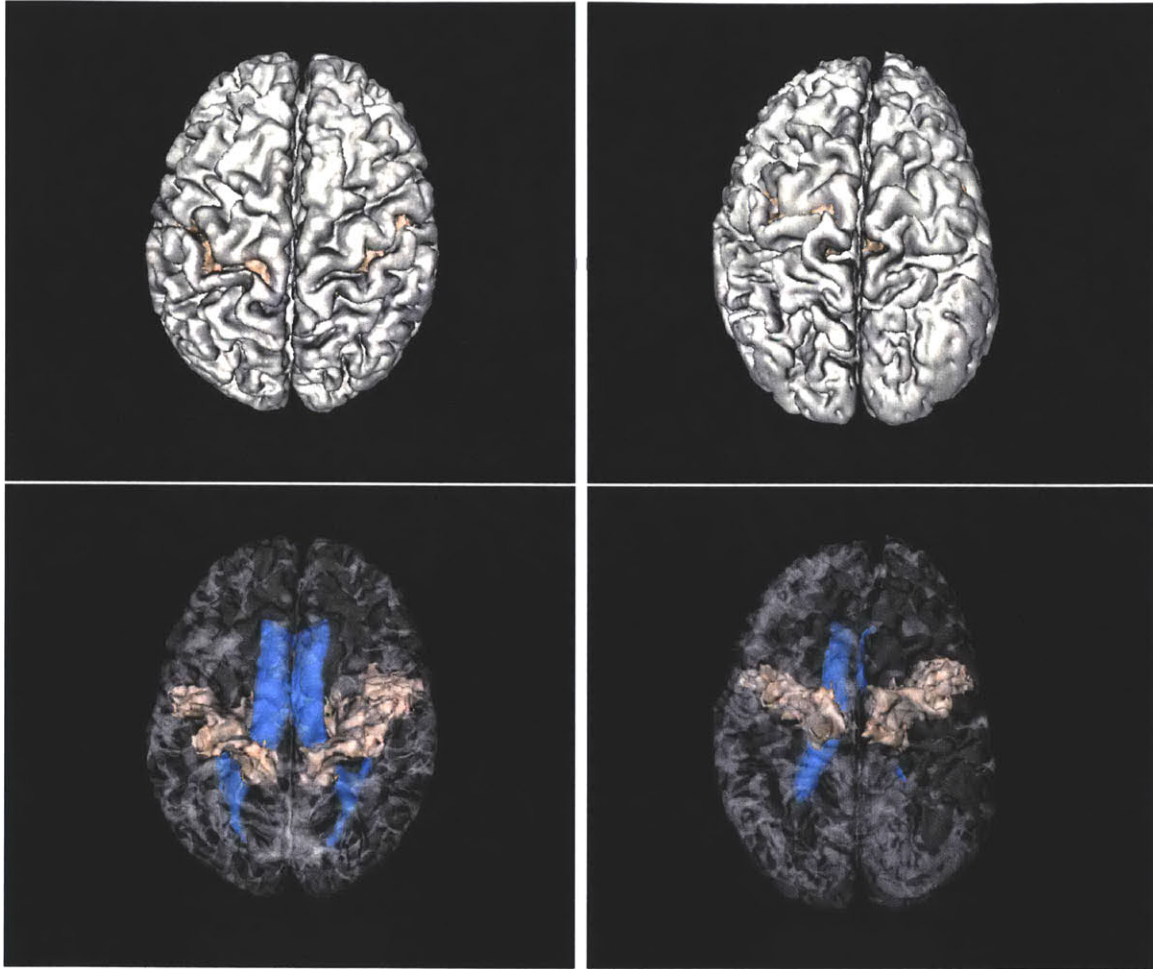


Figure 5-5: Pre- (left) and post-resection (right) models of the brain (white), the ventricles (blue) and the corticospinal tract (pink). The top images present only models of the brain, where the brain shift is very pronounced. The bottom images show the same views with all other models, here it is evident that the tumor was located next to the corticospinal tract.

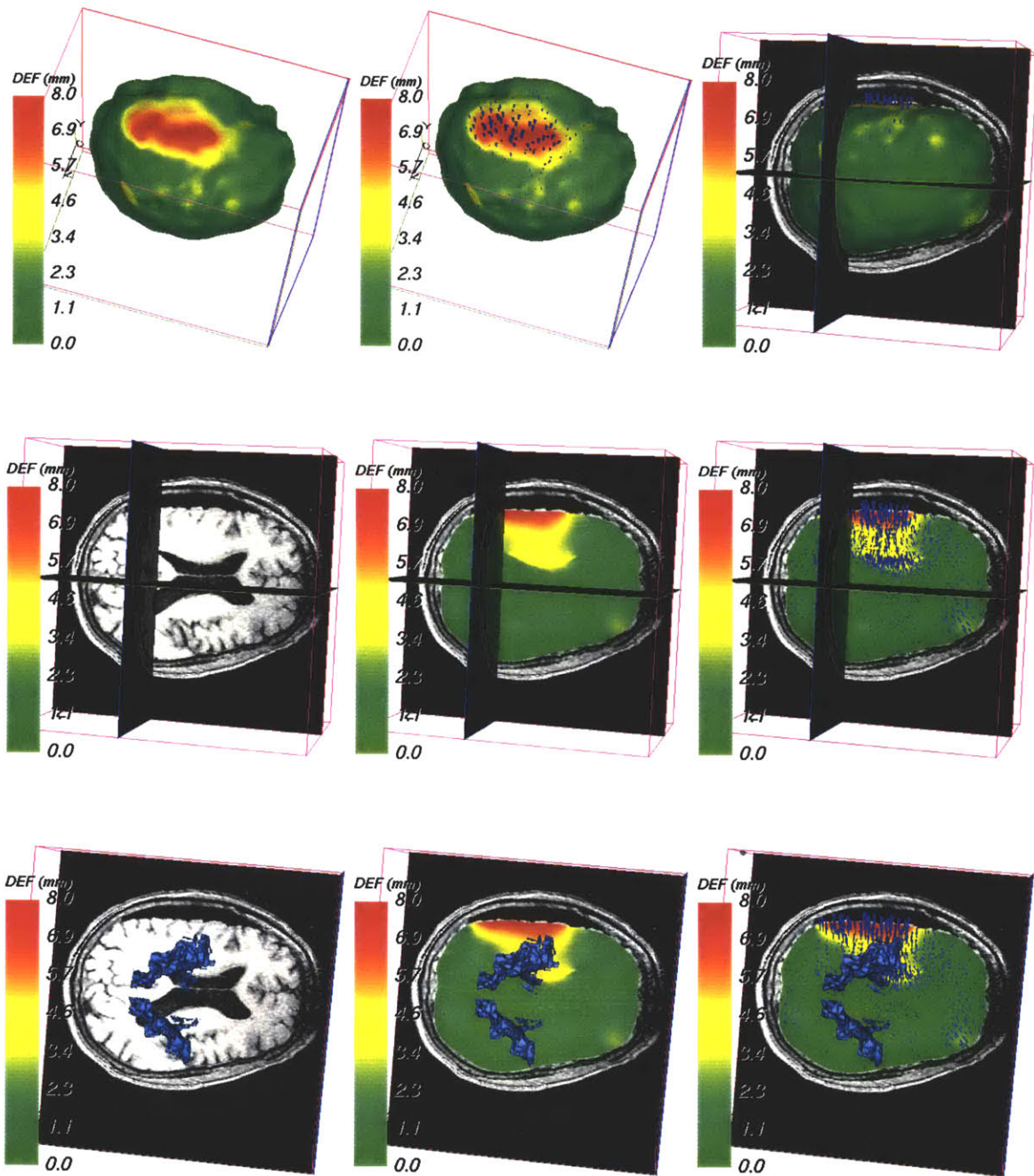


Figure 5-6: Visualization of surface (top) and volumetric deformation fields (middle and bottom) of the first intra-operative scan volume onto the second intra-operative scan volume of the second case. In the bottom images, the volumetric deformation fields are shown aligned with the corticospinal tract (blue). The color-coding indicates the magnitude of the deformation at every point on the surface or cuts of the deformed volume, and arrows indicate the magnitude and direction of the deformation.

studies based on the use of segmented pre-surgical data to create a patient-specific atlas are currently being carried out. The next chapter presents the application of our method to cases where patient's pre-operative MRA data was available, thus it was possible to track vascular structures during IGNS. The fusion of patient-specific multi-modality data provides more accurate intra-operative matches.

# Chapter 6

## Tracking of Vascular Structures during IGNS

### 6.1 Motivation

During a neurosurgical procedure, the tumor is often located in proximity of critical brain structures, which in turn may be accidentally damaged by surgical instruments. In the previous chapter, structures such as the corticospinal tract and the optic radiation were tracked during IGNS procedures by means of a deformable brain atlas. However, such a dataset is generic, i.e. not specific to the patient, which means that some anatomical differences are inevitably present. For this reason, we have created patient-specific datasets by acquiring patient's scans pre-operatively, and then by tracking structures extracted from these datasets during surgery.

This chapter presents a method and the results for the matching of intra-cranial vascular structures, i.e. veins and arteries, extracted from pre-operative MRA data to intra-operative MRI scans. Vascular structures are extracted from pre-surgical PC-MRA scans by means of 3D adaptive filtering and segmentation. Also, such datasets are rigidly registered to other pre-operative scans before surgery. During surgery, these vascular structures are tracked (deformable registration) and visualized in the operating room, so that the surgeon can judge how to progress with the resection.

## 6.2 Description

MRA techniques produce a 3D dataset, which is processed to selectively display the vascular structures of interest. Angiograms based on both phase-contrast [8] and time of flight [38] can be reconstructed from the 3D dataset using a maximum intensity projection, which creates a 2D image by recording the intensity of the brightest voxel along each projection ray through the volume [24]. High-resolution MRA scans often have a high noise level which obscures important diagnostic information in the angiograms [47]. A method to enhance vascular structures and reduce noise in MRA image data, based on the theory of multidimensional adaptive filtering, has been developed by Westin et al. [47]. This technique is based on local structure estimation using six 3D orientation selective filters and adaptive filtering controlled by the local structure information.

Our surgical case presented a left posterior temporal low-grade oligodendroglioma, of which great part was removed during surgery. Models of arteries (red) and veins (blue), extracted from the pre-surgical MR angiogram and rigidly registered to the pre-operative SPGR scan, are presented in Figure 6-1. The top image displays only the models, while the bottom image shows the same view but together with orthogonal cuts of the pre-operative SPGR acquisition.

Our method for tracking arterious and veneous brain structures is based on the acquisition and filtering of the patients MRA dataset, followed by a segmentation step which is carried out using thresholding and manual correction provided by the 3D slicer [15]. Since many different scans are acquired before surgery, they all need to be rigidly registered. We normally register a PC-MRA scan to a T1-weighted, SPGR volume of the same patient using the method described in [46]. Together with the phase-contrast scan, an intensity based scan is also acquired during the usual MRA acquisition at the BWH (following the *Protocol 55* procedure). This dataset is used when rigidly registering the angiogram to the SPGR, as they contain similar anatomical information on the brain.

These steps can be time consuming, but they are all carried out before surgery,

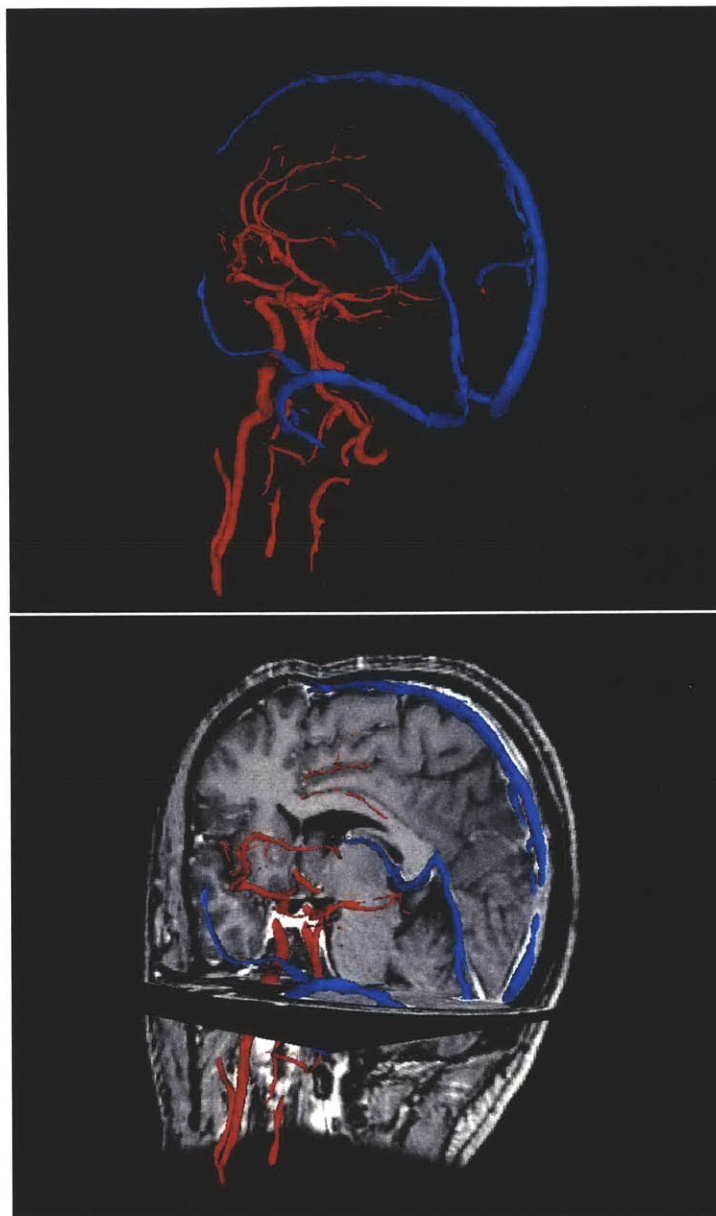


Figure 6-1: Models of arteries (red) and veins (blue) rigidly registered to the pre-operative SPGR scan (shown in the bottom figure).

as the data is already available. During surgery, the methodology we used is the same as described in Chapters 2, 3 and 4, with the pre-operative data being the MR angiogram. Results of some initial experiments carried out retrospectively are shown in the next section. Since vascular structures are usually very thin, the resampling steps following the pre- and intra-procedural registration of vessels data to MR images turned out to require extra processing time. However, the intra-operative timing of such experiments did not exceed 15 minutes, which demonstrates the feasibility and the usefulness of our method during neurosurgery. Such work is currently being carried out at the SPL.

### 6.3 Results

A rigid registration of arteries and veins to an intra-operative scan was shown in Figure 4-1, where models of arteries and veins extracted from the pre-operative PC-MRA dataset were shown together with models of brain and residual tumor extracted from the MRI scan acquired during surgery. Here we present results for the non-rigid case, where the FE biomechanical model was used to obtain the deformation fields from intra-operatively acquired scans and applied them to pre-surgical images.

Figure 6-2 shows models of arteries (red) and veins (blue) resulting from the non-rigid registration of MRA data onto an intra-operative SPGR acquired after some degree of resection (also shown in the picture). The registration was accurate and provided useful information for surgical planning. It can be noticed in Figure 6-2 that the arteries in proximity of the resection cavity were registered correctly as they overlap with the flow voids present in the intra-operative MR image. In a brain SPGR acquisition, these flow voids correspond to vascular structures and are thus a useful and reliable landmark for validation purposes.

In spite of the accuracy of the registration, the quality of the models is not as good as for the cases presented in Chapter 5, because of the thin nature of vascular structures, which are in turn greatly affected each time the data is resampled. In ideal circumstances, resampling would not be needed. Also, in this case the tumor was not

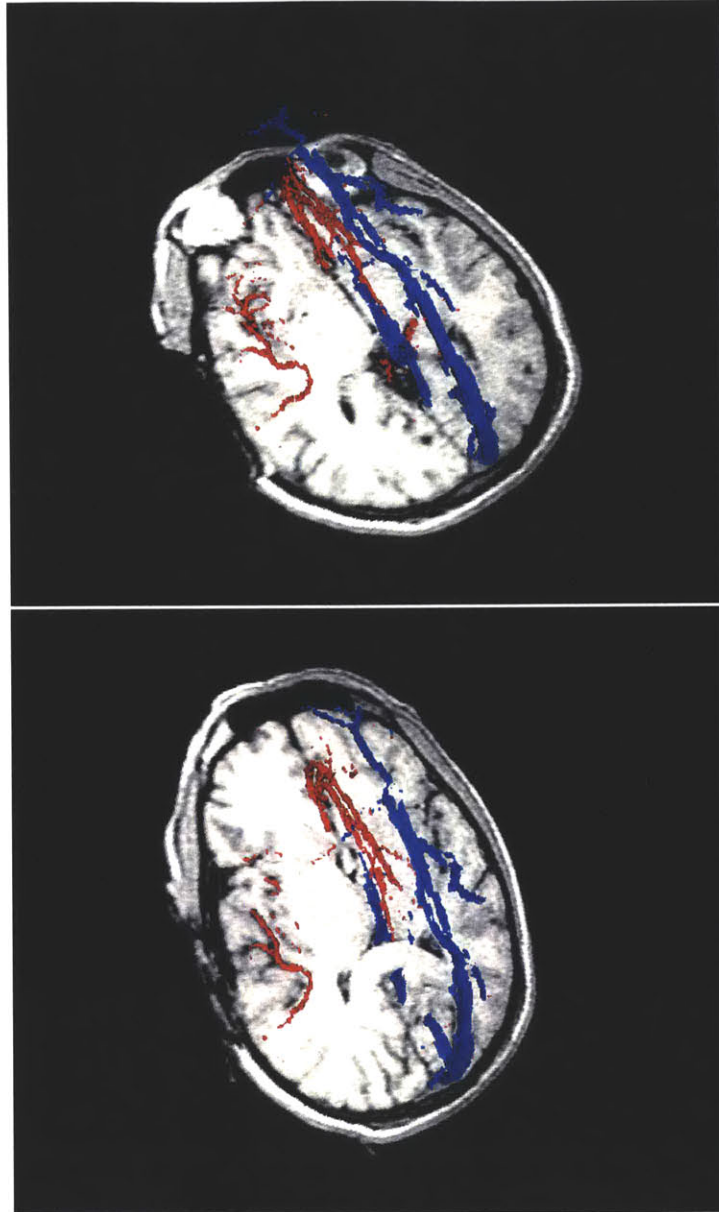


Figure 6-2: Models of arteries (red) and veins (blue) deformed onto an intra-operative SPGR image acquired after some degree of resection and also shown in the picture. Note that the arteries in proximity of the resection cavity overlap with the flow voids present in the intra-operative MR image.



located particularly close to any major vessel, only a few arteries were located near the resection site, so the non-rigid registration has not been as useful as for other situations. However, in some neurosurgical procedures the tumor can be located in close anatomical relationship to major vessels, thus in such cases it is important to track these structures during the resection.

# Chapter 7

## Tracking of Cortical Structures during IGNS

### 7.1 Motivation

In Chapter 6, our method for intra-operative matching was applied to pre-surgical MRA data. Similarly, in this chapter a surgical case where a patient's pre-operative fMRI scan was non-rigidly matched to intra-operative images is presented. The motivation behind the employment of this modality is that neurosurgical cases would normally benefit from the tracking of cortical structures extracted from fMRI acquisitions more often than from the tracking of vascular structures extracted from MR angiograms, as tumors are rarely located in proximity of a major vessel.

Functional MRI is a recently discovered technique used to measure the quick, small metabolic changes that take place in an active part of the brain. This imaging method provides high-resolution, non-invasive reports of neural activity detected by a blood oxygen level dependent signal, and can be very useful in neurosurgical practice. Currently, it is not feasible to acquire fMRI sequences during a surgical case. However, our method can provide the surgeon with comparable, as well as reliable information by matching pre-operative fMRI data during an IGNS procedure.

## 7.2 Description

In cases where the patient's pathology is located near the motor cortex, functional MR scans are usually acquired pre-surgically. The fMRI technique determines which parts of the brain are activated by different types of physical sensation or activity, such as sight, sound or the movement of a subject's fingers. This "brain mapping" is achieved by setting up an advanced MRI scanner in a special way so that the increased blood flow to the activated areas of the brain shows up on fMRI scans. One mechanism depends upon the fact that the microvascular MR signal on T2-weighted images is strongly influenced by the oxygenation state of the blood, also known as Blood Oxygenation Level Dependent or "BOLD" effect that can be observed by non-invasive MR imaging at high magnetic fields [3].

During a pre-surgical image acquisition, a high resolution single scan is taken first, which is used later as a background for highlighting the brain areas which were activated by the stimulus. Then, a series of low resolution scans is taken over time; for some of these scans, the stimulus is present, while for other scans, the stimulus is absent. The low-resolution brain images in the two cases can be compared, in order to see which parts of the brain were activated by the stimulus. The final statistical image shows up bright in those parts of the brain, which were activated by this experiment, then shown as colored blobs on top of the original high resolution scan.

In our surgical case, these colored blobs corresponded to areas of activation of hand functions (activated by a finger tapping task during the fMRI acquisition). The patient had a small tumor involving the premotor (supplementary motor area) and partially the motor cortex. Only the anterior part of the tumor was removed, while the portion which involved the motor strip was left in place. During surgery, the patient got a motor deficit of the right hand and wrist, which improved in the following hours (the so-called "supplementary motor area syndrome"). The brain shift was visible, though not marked.

Figure 7-1 shows pre-surgical fMRI images. The top pictures show models of the brain (white), the ventricles (blue), the tumor (green), and the fMRI activation areas

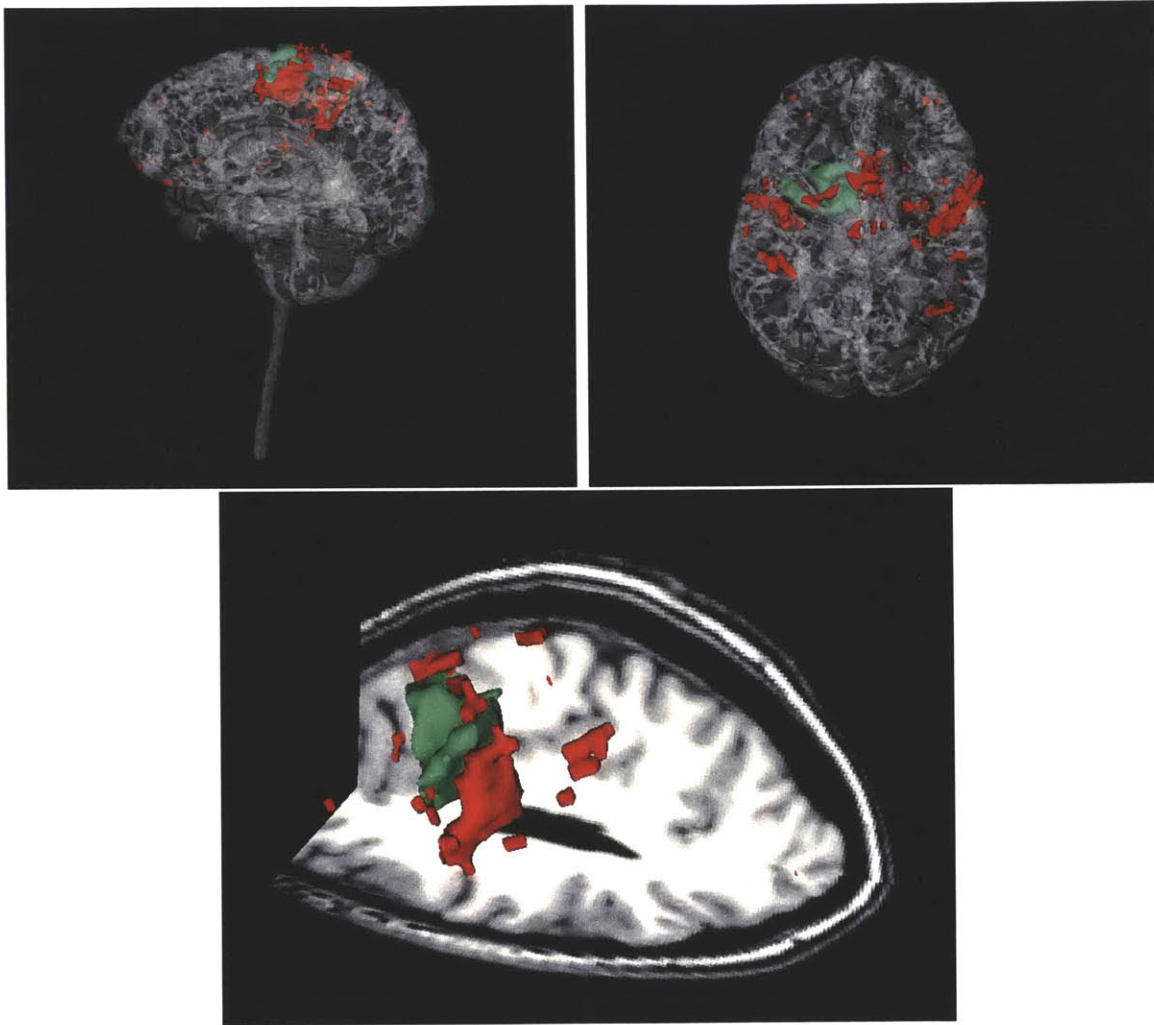


Figure 7-1: Top: Models of the brain (white), the ventricles (blue), the tumor (green), and the fMRI activation areas (red) extracted from the pre-operative fMRI scan. Bottom: Models of the tumor and fMRI activation areas shown along with the pre-surgical SPGR image provide a closer look at the region near the tumor. The strong anatomical relationship of the tumor and the hand movement control areas can be clearly noticed.

(red) extracted from the pre-operative fMRI scan. The bottom picture provides a closer look at the region near the tumor by displaying models of the tumor and fMRI activation areas shown along with the pre-surgical SPGR image. The strong anatomical relationship of the tumor and the hand movement control areas can be clearly noticed. In such case, the neurosurgeon has to be extremely careful in not damaging those areas when resecting the tumor. However, these images allow the neurosurgeon to plan the procedure accordingly.

The fMRI activation areas were segmented pre-surgically using the 3D slicer [15]. Next, the fMRI image was rigidly registered to other pre-operative acquisitions, such as SPGR, T2-weighted and diffusion scans, using the MI-based method presented in [46]. During surgery, the methodology we used was the same as described in Chapters 2, 3 and 4, with the pre-operative data being the functional MR scan.

Results of some initial experiments carried out retrospectively are shown in the next section. The intra-operative timing of such experiments was below 12 minutes, since fMRI cases require the same amount of processing as the atlas matching cases (on the other hand, MRA cases are more time demanding due to the unique processing of thin vascular structures). This demonstrates the usefulness of our method also in the case of functional MR imaging. Experiments of such technique, carried out prospectively during IGNS, are currently a strong research interest at the SPL.

## 7.3 Results

Intra-operative results are shown in Figure 7-2, which displays models of the brain (white), the ventricles (blue), and the fMRI activation areas (yellow) extracted from the pre-operative scan after matching it to an intra-operative image acquired after some degree of resection. The bottom picture also displays a slice of the intra-operative SPGR scan.

Figure 7-3 presents a 2D axial view of pre- and intra-operative grayscale MR images overlaid such that the pre-operative is shown with a threshold (yellow-green) in order to visualize the direction of the brain shift. Since it is difficult to compare

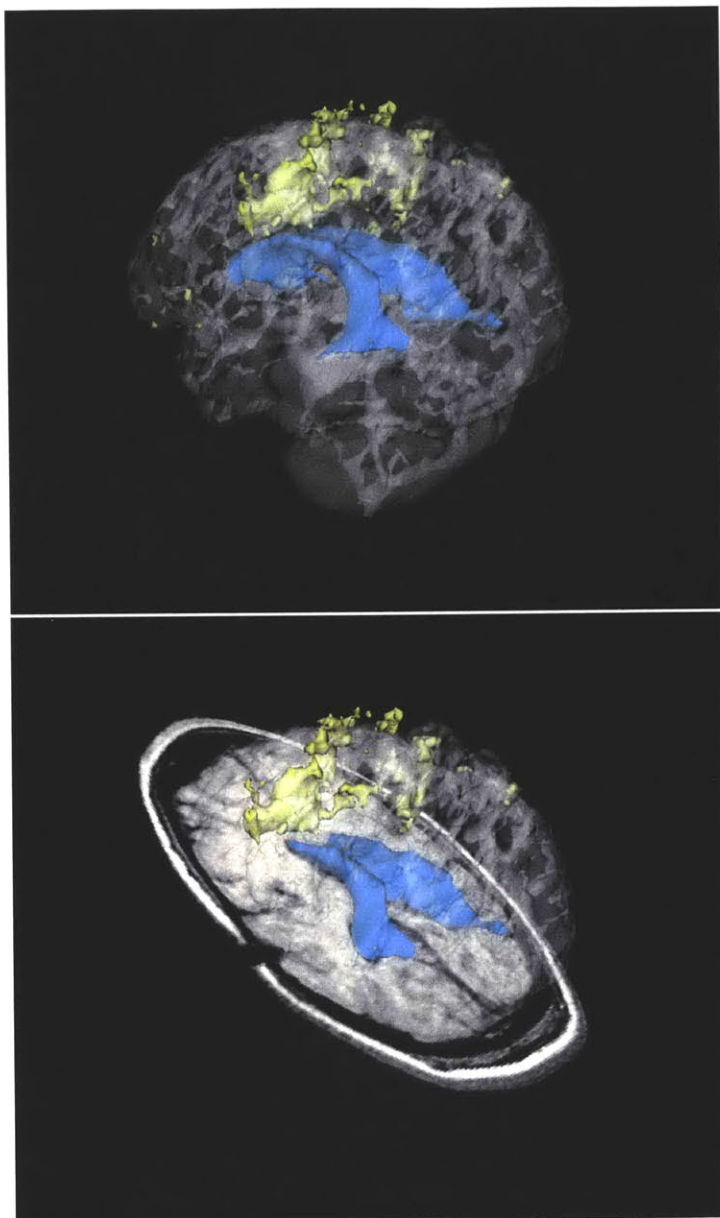


Figure 7-2: Models of the brain (white), the ventricles (blue), and the fMRI activation areas (yellow) extracted from the pre-operative scan after matching it to an intra-operative image acquired after some degree of resection. The bottom picture also displays a slice of the intra-operative SPGR scan.

two T1-weighted grayscale images by simply overlaying them, the pre-surgical scan was thresholded such that its contours are clearly visible on top of the intra-operative image. By looking at the whole brain, one can notice that the left part has not shifted much, as the pre- and intra-operative sulci still overlap consistently. On the other hand, as the tumor was located towards the middle of the right side of the brain, this part has shifted in two directions. The part above the tumor has shifted posteriorly, while the part below the tumor has shifted anteriorly. As an example, red arrows show that the central sulcus has shifted anteriorly by a few millimeters.

Models of the brain (blue), the tumor resection cavity (white), pre-operative fMRI activation areas (red), and the fMRI activation areas extracted from the pre-operative scan after matching it to an intra-operative image acquired after some degree of resection (yellow) are shown in Figure 7-4. This view is opposite to that of Figure 7-3 such that the brain shift is on the left. One can notice the significant difference between the fMRI activation areas extracted from the pre-surgical scan and those extracted from that scan deformed onto the intra-operative MR image. Such difference may be critical for the surgical outcome, thus it is very important to track these brain structures during neurosurgery.

In conclusion, a visual inspection of the non-rigid registration shows that it was indeed very accurate and therefore provided useful information for neurosurgical planning. More cases need to be carried out in order to fully validate this method. However, both this and the MRA case (see Chapter 6) were the first attempts of applying a non-rigid technique for the intra-operative tracking of patient-specific multi-modality datasets. The results presented here and in the previous chapter show the great potential of the method described in this thesis for the real-time tracking of critical brain structures during IGNS procedures.

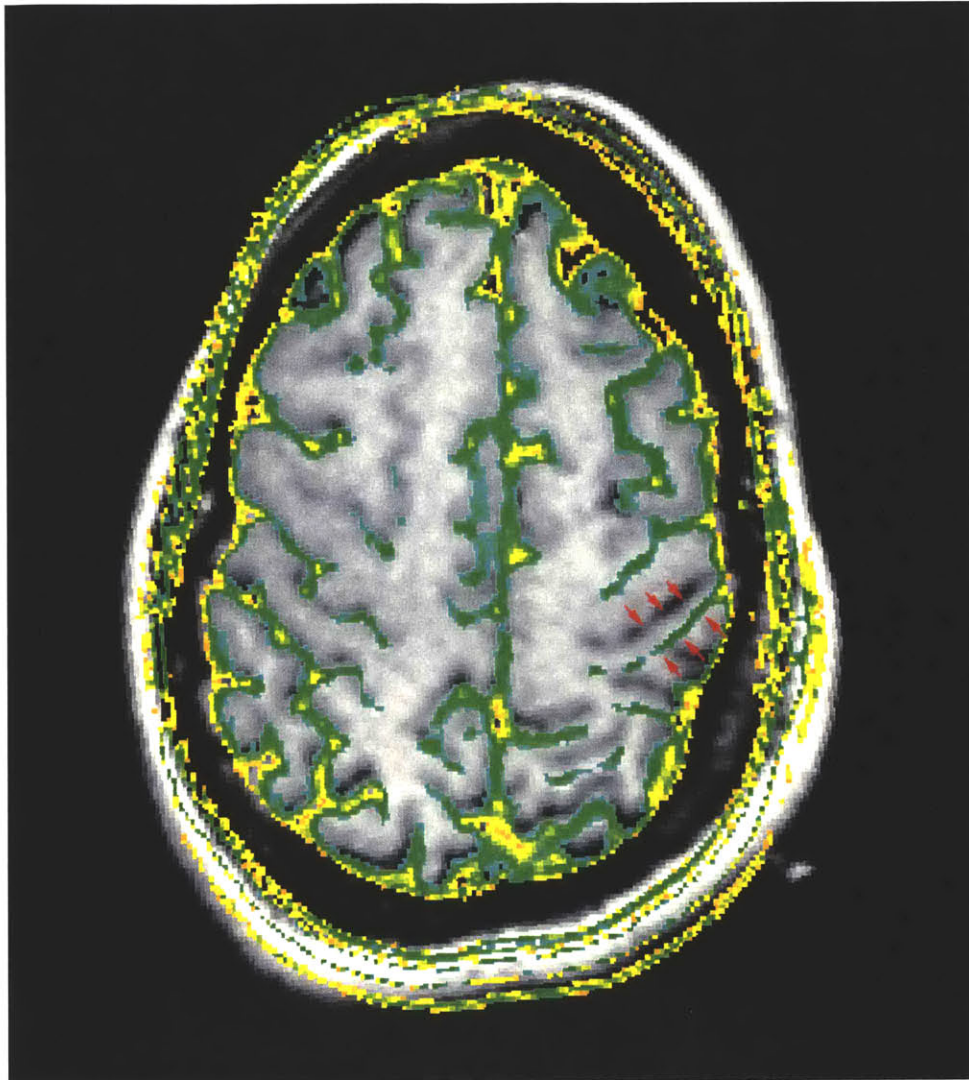


Figure 7-3: 2D axial view of pre- and intra-operative grayscale MR images overlaid such that the pre-operative is shown with a threshold (yellow-green) in order to visualize the direction of the brain shift. Red arrows show that the central sulcus has shifted anteriorly by a few millimeters.



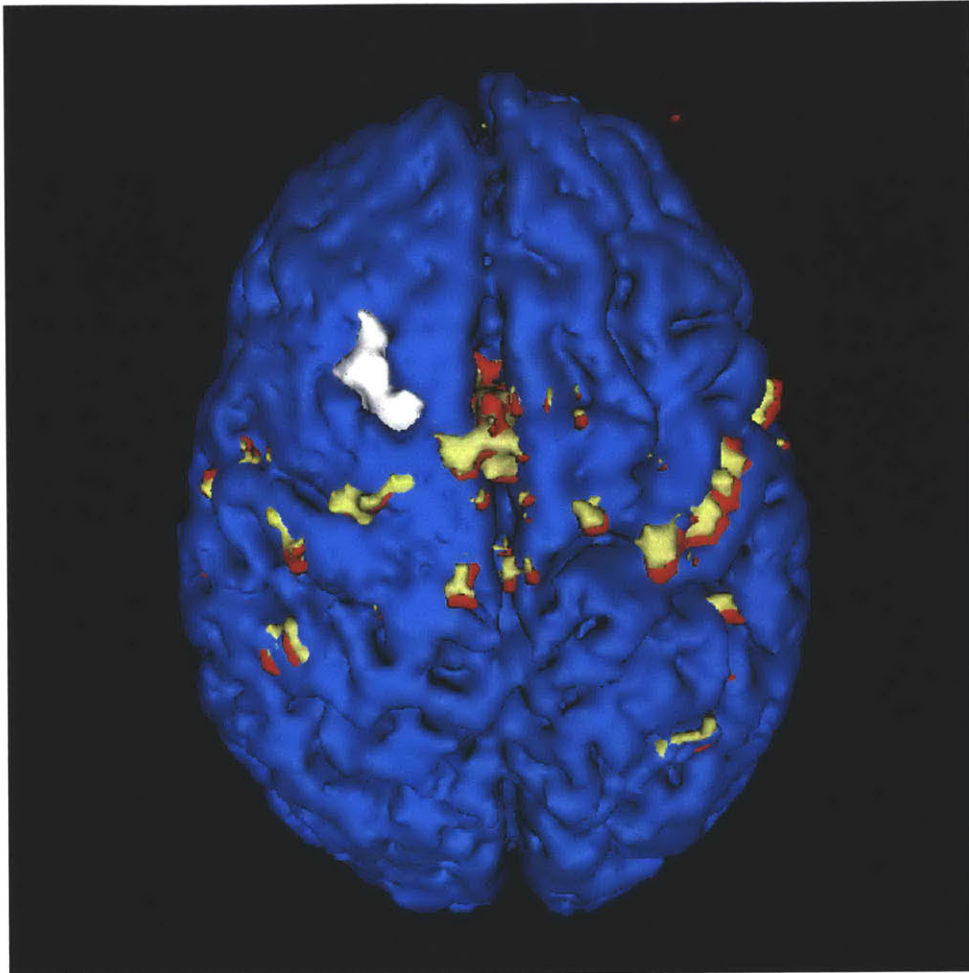


Figure 7-4: Models of the brain (blue), the tumor resection cavity (white), pre-operative fMRI activation areas (red), and the fMRI activation areas extracted from the pre-operative scan after matching it to an intra-operative image acquired after some degree of resection (yellow).

# Chapter 8

## Conclusions and Future Work

### 8.1 Discussion of Results

A physics-based biomechanical model provided the means to accurately capture the volumetric deformation the brain undergoes during neurosurgery and the application of this deformation to several image datasets allowed for the fusion of multi-modality image data. Real-time tracking of critical brain structures during IGNS was shown in three different situations:

1. A generic volumetric brain atlas was deformed intra-operatively during some neurosurgical cases, and provided additional information on structures (such as the corticospinal tract and the optic radiation), that were critical for each specific case. These experiments were performed during the procedures, in order to demonstrate the real-time capabilities of the method presented in this thesis, but, due to the employment of a generic atlas, did not attempt to provide an accurate description of the patient's anatomy.
2. Brain vascular structures (i.e. arteries and veins), extracted from a pre-surgical patient-specific MRA scan, were deformed onto intra-operatively acquired images. While the match to the patient's anatomy was very accurate, this first test was performed retrospectively and required some extra computing time due to the special processing needed by the thin nature of the vessels. However, the

timing was still feasible for future intra-surgical employment of this method.

3. Brain cortical structures, corresponding to the activation areas (of hand functions) of a patient-specific pre-operative fMRI scan, were also deformed onto images acquired intra-operatively. Again, the match to the patient's anatomy was very accurate. Although this first test was performed retrospectively, the timing was as good as for the atlas matching cases which makes it very feasible to employ this method for future neurosurgical procedures.

These results show that tracking volumetric brain deformations intra-operatively and using them to match multi-modality pre-operative data during IGNS procedures can improve the information-content of the images visualized by the surgeon in the operating room.

## 8.2 Major Achievements and Contributions

This thesis was driven by the belief that non-rigid registration through a physics-based model could accurately capture the deformation of the brain during neurosurgical procedures. The final aim was to apply this deformation to pre-operatively acquired data so the visualization environment available during surgery could be improved. The display of multi-modality image data could then provide the surgeon with useful information from which to determine the course of the tumor resection.

Therefore, the major contributions of this work are:

- A prospective evaluation of a FE based biomechanical model for the purpose of deformable registration of brain images during IGNS procedures. This method meets the real-time constraints of neurosurgery through the application of fast HPC algorithms.
- A proof of the concept that multi-modality registration is feasible during IGNS procedures, in particular using MRA and fMRI pre-operative scans, from which critical brain structures can be visualized during surgery.

- A reliable improvement of the information-content of intra-operatively acquired images by the tracking of volumetric brain deformation (accounting for the “brain shift”) when mapping pre-operative data during neurosurgery. This is a major step forward, as previously it was possible to only rigidly register image data during a surgical procedure.

### 8.3 Perspectives and Future Work

In Chapter 5, we showed that it is possible to track anatomical structure extracted from a generic deformable brain atlas and that the method presented in this thesis is fast enough to be practical for clinical use during neurosurgery. In Chapters 6 and 7, we also showed two cases where patient’s angiography and fMRI data were matched to intra-operative neurosurgical images. However, these latter cases were performed retrospectively to demonstrate the clinical usefulness of the method proposed in this thesis. More rigorous prospective validation studies, using segmented pre-operative MRA and fMRI data to create a patient-specific atlas, are currently being conducted at the SPL. In the future, it would be desirable to also incorporate diffusion tensor images to better visualize white matter tracts.

As computers continue to get faster and computing resources continue to quickly improve over time, the algorithms used in this thesis will be even more efficient. When more CPU’s will be available the time required by the deformable registration will decrease accordingly. However, this part of the method has already been optimized and, although it is the most computational demanding, it is also the fastest. Some algorithmic improvements would be eventually required by the segmentation and the rigid registration techniques.

For instance, image segmentation algorithms, which are currently used to identify key surfaces for the biomechanical simulation of deformation, rely upon image signal intensities. A strong model of the prior probability of the spatial distribution of brain and ventricles would help to improve the robustness and the speed of the image segmentation. Such a model could be derived by aligning large numbers of subjects

scans and then measuring the empirical distribution of tissue classes.

Another future aim would be to expand the biomechanical model to incorporate an anisotropic inhomogeneous white matter material model, and include a nonlinear, potentially hyper-viscoelastic framework. Intra-operative measurements of brain material properties are planned to be performed at the SPL in the near future. For instance, it will be possible to measure the pressure applied by the surgeon with the retractor. Such physiological parameters could be then included in our modeling system, which in turn would become more physiologically significant.

We expect that the fusion of patient-specific multi-modality data and the use of an improved biomechanical model will provide more accurate intra-operative matches during neurosurgery procedures. This method has the potential to increase the information-content of intra-operative images and to enable an accurate description of surgical changes.

# Appendix A

## Glossary of Abbreviations

<b>2D</b>	Two-Dimensional
<b>3D</b>	Three-Dimensional
<b>BOLD</b>	Blood Oxygenation Level Dependent
<b>BWH</b>	Brigham and Women's Hospital
<b>CT</b>	Computed Tomography
<b>CTA</b>	Computed Tomography Angiography
<b>DSA</b>	Digital Subtraction Angiography
<b>DTMRI</b>	Diffusion Tensor Magnetic Resonance Imaging
<b>FE</b>	Finite Element
<b>fMRI</b>	Functional Magnetic Resonance Imaging
<b>FSE</b>	Fast Spin Echo (T2-weighted MR acquisition)
<b>HPC</b>	High-Performance Computing
<b>IGNS</b>	Image-Guided Neurosurgery
<b>MI</b>	Mutual Information
<b>MPI</b>	Message Passing Interface
<b>MR</b>	Magnetic Resonance
<b>MRA</b>	Magnetic Resonance Angiography
<b>MRI</b>	Magnetic Resonance Imaging
<b>MRT</b>	Magnetic Resonance Therapy
<b>PC-MRA</b>	Phase-Contrast Magnetic Resonance Angiography
<b>PET</b>	Positron Emission Tomography
<b>PETSc</b>	Portable, Extensible Toolkit for Scientific Computation
<b>SMP</b>	Symmetric Multiprocessor
<b>SPECT</b>	Single Photon Emission Computed Tomography
<b>SPGR</b>	Spoiled Gradient Echo (T1-weighted MR acquisition)
<b>SPL</b>	Surgical Planning Laboratory
<b>US</b>	Ultrasound

Table A.1: Glossary of Abbreviations.

## Appendix B

# Computational Facilities at the Surgical Planning Laboratory

The SPL is a computational facility totally integrated into the clinical environment, being immediately adjacent to several active operating rooms at the BWH. Also, the Radiology department's main MRI and CT scanners are very closely located; data from these scanners is available directly from the SPL's network. The center of the SPL's high-speed network is an Alcatel 7020/Omnicores 5052 enterprise-class routing switch, capable of managing the traffic from hundreds of 10 or 100 MB/Sec Fast Ethernet and scores of 1GB/sec Gigabit Ethernet connections. This central switch services direct connections from the machines in the SPL's central computer facility, including approximately 50 workstations and laptops, and connects directly to the offices in the Thorn research building, the open magnet MR system in the MRT operating room, and the Center for Neurologic Imaging.

The UNIX Workstations, such as Sun Ultra 10 with Creator 3D or Elite 3D graphics cards, are the most ordinarily used computational tools. A picture of a cluster of Sun Microsystems machines is shown in Figure B-1. For more demanding tasks, one can access several Ultra80 workstations (shown in Figure B-2), each with 4 processors and about 4 GB of RAM. The SPL's high performance computing system is made up of a variety of enterprise-class SMP computers from Sun Microsystems. These machines include two ES5000 machines (shown in Figure B-3), each with 8

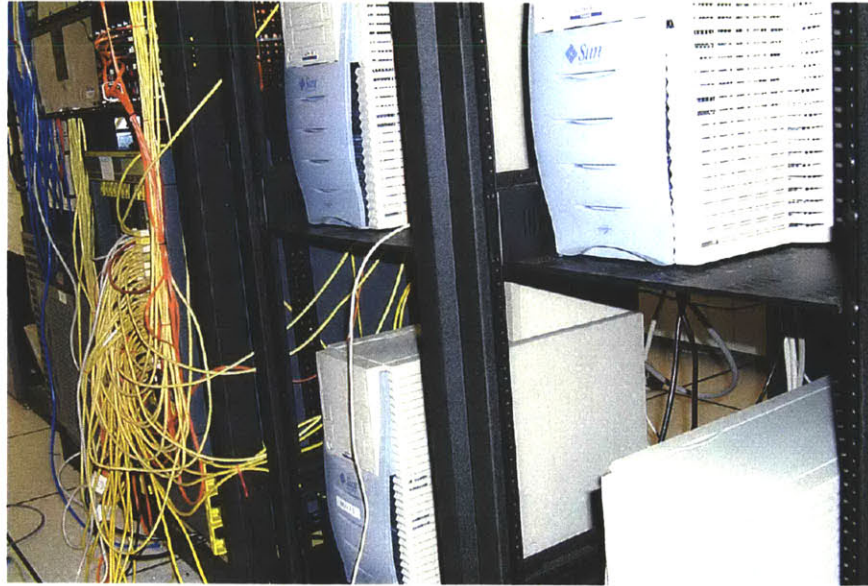


Figure B-1: Cluster of Sun Microsystems computers.

processors and 2GB of RAM, and one ES6000 with 18 processors and 5GB of RAM. Recently, two Sun Fire 6800 with 12 750MHz UltraSPARC-III CPU's and 12 GB of RAM have been added. In addition to these machines, a 4 CPU's Sun ES450 application and file server is available to take the more commonplace computational load off the larger machines. The file server is shown in Figure B-4.

A high reliability network attached storage device from Procom Technology is also available. The Procom NetForce 3100 holds 2.5 Terabytes of data using redundant FibreChannel disk arrays and a specialized disk computer (filter head). A 2 Gigabit Ethernet links directly to the network switch and permits individual client machines to write data at up to 30 MB/sec [34].





Figure B-2: Sun Microsystems workstation (Ultra 80).



Figure B-3: Sun Microsystems SMP machine (Enterprise 5000).

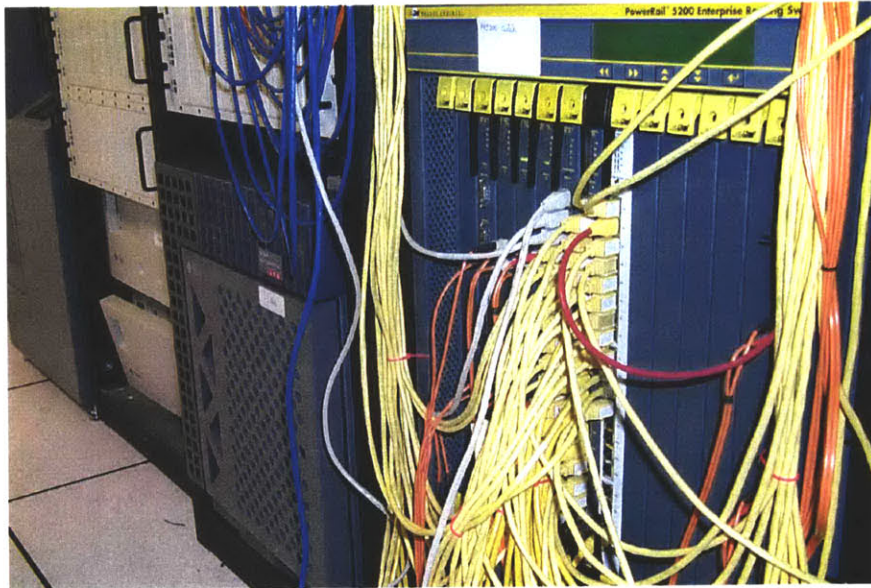


Figure B-4: Sun Microsystems file server.

# Bibliography

- [1] S. Balay, W. D. Gropp, L. Curfman McInnes, and B. F. Smith. Efficient management of parallelism in object oriented numerical software libraries. In E. Arge, A. M. Bruaset, and H. P. Langtangen, editors, *Modern Software Tools in Scientific Computing*, pages 163–202. Birkhauser Press, 1997.
- [2] S. Balay, W. D. Gropp, L. Curfman McInnes, and B. F. Smith. PETSc 2.0 users manual. Technical Report ANL-95/11 - Revision 2.0.28, Argonne National Laboratory, 2000.
- [3] J.W. Belliveau, D.N. Kennedy, and R.C Mckinstry. Functional mapping of the human visual cortex by magnetic resonance imaging. *Science*, 254:716–719, 1991.
- [4] P. McL. Black, E. Alexander, C. H. Martin, T. Moriarty, A. Nabavi, T. Z. Wong, R. B. Schwartz, and F. A. Jolesz. Craniotomy for Tumor Treatment in an Intraoperative Magnetic Resonance Imaging Unit. *Neurosurgery*, 45:423–433, 1999.
- [5] M. Bro-Nielsen. Surgery Simualation Using Fast Finite Elements. *Visualization in Biomedical Computing*, pages 529–534, 1996.
- [6] L. Cohen and I. Cohen. Finite Element Methods for Active Contour Models and Balloons for 2D and 3D Images. *IEEE Transactions on Pattern Analysis and Machine Intelligence*, 15:1131–1147, 1993.

- [7] O. Cuisinaire and B. Macq. Fast Euclidean Distance Transformation by Propagation Using Multiple Neighborhoods. *Computer Vision and Image Understanding*, 76:163–172, 1999.
- [8] C. L. Dumoulin, S. P. Souza, M. F. Walker, and W. Wagle. Three-Dimensional Phase Contrast MR Angiography. *Magnetic Resonance in Medicine*, 9:139–149, 1989.
- [9] P. J. Edwards, D. L. G. Hill, J. A. Little, and D. J. Hawkes. Deformation for Image Guided Interventions Using a Three Component Tissue Model. In *Proceedings of International Conference of Information Processing in Medical Imaging*, pages 218–231, 1997.
- [10] M. Ferrant. *Physics-based Deformable Modeling of Volumes and Surfaces for Medical Image Registration, Segmentation and Visualization*. PhD thesis, Louvain, Belgium: Universite’ Catholique de Louvain, 2001.
- [11] M. Ferrant, A. Nabavi, B. Macq, P. McL. Black, F. A. Jolesz, R. Kikinis, and S. K. Warfield. Serial Registration of Intraoperative MR Images of the Brain. *Medical Image Analysis*, 2001. In Press.
- [12] M. Ferrant, A. Nabavi, B. Macq, F. A. Jolesz, R. Kikinis, and S. K. Warfield. Registration of 3D Intraoperative MR Images of the Brain Using a Finite Element Biomechanical Model. *IEEE Transactions On Medical Imaging*, 2001.
- [13] M. Ferrant, S. K. Warfield, A. Nabavi, B. Macq, and R. Kikinis. Registration of 3D Intraoperative MR Images of the Brain Using a Finite Element Biomechanical Model. In *MICCAI 2000: Third International Conference on Medical Robotics, Imaging And Computer Assisted Surgery; 2000 Oct 11–14; Pittsburgh, USA*, pages 19–28, Heidelberg, Germany, 2000. Springer-Verlag.
- [14] B. Geiger. Three-dimensional modeling of human organs and its application to diagnosis and surgical planning. Technical Report 2105, INRIA, 1993.

- [15] D. T. Gering, A. Nabavi, R. Kikinis, N. Hata, L. J. O'Donnell, W. E. Grimson, F. A. Jolesz, P. McL. Black, and W. M. Wells III. An Integrated Visualization System for Surgical Planning and Guidance Using Image Fusion and an Open MR. *Journal of Magnetic Resonance Imaging*, 13:967–975, 2001.
- [16] A. Hagemann, K. Rohr, H. S. Stiel, U. Spetzger, and J. M. Gilsbach. Biomechanical modeling of the human head for physically based, non-rigid image registration. *IEEE Transactions On Medical Imaging*, 18(10):875–884, 1999.
- [17] N. Hata. *Rigid and Deformable Medical Image Registration for Image-Guided Surgery*. PhD thesis, University of Tokyo, 1998.
- [18] N. Hata, A. Nabavi, W. M. Wells, S. K. Warfield, R. Kikinis, P. M. Black, , and F. A. Jolesz. Three-Dimensional Optical Flow Method for Measurement of Volumetric Brain Deformation from Intraoperative MR Images. *J Comput Assist Tomogr*, 24:531–538, 2000.
- [19] D. Hill, C. Maurer, R. Maciunas, J. Barwise, J. Fitzpatrick, and M. Wang. Measurement of Intraoperative Brain Surface Deformation Under a Craniotomy. *Neurosurgery*, 43:514–526, 1998.
- [20] F. A. Jolesz. Image-guided procedures and the operating room of the future. *Radiology*, 204:601–612, 1997.
- [21] M. Kass, A. Witkin, and D. Terzopoulos. Snakes: Active Contour Models. *International Journal of Computer Vision*, 1:321–331, 1988.
- [22] M. R. Kaus, A. Nabavi, C. T. Mamisch, W. M. Wells, F. A. Jolesz, R. Kikinis, and S. K. Warfield. Simulation of Corticospinal Tract Displacement in Patients with Brain Tumors. In *MICCAI 2000: Third International Conference on Medical Robotics, Imaging And Computer Assisted Surgery; 2000 Oct 11-14; Pittsburgh, USA*, pages 9–18, Heidelberg, Germany, 2000. Springer-Verlag.
- [23] R. Kikinis, M. E. Shenton, D. V. Josifescu, R. W. Carley, P. Saiviroonporn, H. H. Hokama, A. Robatino, D. Metcalf, C. G. Wible, C. M. Portas, R. M.

- Donnino, and F. A. Jolesz. A Digital Brain Atlas for Surgical Planning, Model Driven Segmentation, and Teaching. *IEEE Transactions on Visualization and Computer Graphics*, 2:232–241, 1996.
- [24] G. Laub. Displays for MR Angiography. *Magnetic Resonance in Medicine*, 14:222–229, 1990.
- [25] M. I. Miga, K. D. Paulsen, J. M. Lemery, A. Hartov, and D. W. Roberts. In vivo quantification of a homogeneous brain deformation model for updating preoperative images during surgery. *IEEE Transactions On Medical Imaging*, 47(2):266–273, 1999.
- [26] M. I. Miga, D. W. Roberts, F. E. Kennedy, L. A. Platenik, A. Hartov, K. E. Lunn, and K. D. Paulsen. Modeling of Retraction and Resection for Intraoperative Updating of Images. *Neurosurgery*, 49:75–85, 2001.
- [27] K. Miller and K. Chinzei. Constitutive modelling of brain tissue: experiment and theory. *Journal of Biomechanics*, 30(11–12):1115–1121, 1997.
- [28] K. Miller, K. Chinzei, G. Orssengo, and P. Bednarz. Mechanical properties of brain tissue in-vivo: experiment and computer simulation. *Journal of Biomechanics*, 33(11):1369–1376, 2000.
- [29] A. Nabavi, P. McL. Black, D. T. Gering, C. F. Westin, V. Mehta, R. S. Pergolizzi, M. Ferrant, S. K. Warfield, N. Hata, R. B. Schwartz, W. M. Wells III, R. Kikinis, and F. A. Jolesz. Serial Intraoperative MR Imaging of Brain Shift. *Neurosurgery*, 48:787–798, 2001.
- [30] G. Nielson and J. Sung. Interval volume tetrahedrization. *Visualization '97, IEEE*, 1997.
- [31] K. D. Paulsen, M. I. Miga, F. E. Kennedy, P. J. Hoopes, A. Hartov, and D. W. Roberts. A Computational Model for Tracking Subsurface Tissue Deformation During Stereotactic Neurosurgery. *IEEE Transactions On Medical Imaging*, 47(2):213–225, 1999.

- [32] T. Rohlfing and C. R. Maurer. Intensity-based Non-Rigid Registration Using Adaptive Multilevel Free-Form Deformation with an Incompressibility Constraint. In *MICCAI 2001: Fourth International Conference on Medical Robotics, Imaging And Computer Assisted Surgery; 2001 Oct 14-17; Utrecht, the Netherlands*, pages 111–119, Berlin Heidelberg, Germany, 2001. Springer-Verlag.
- [33] W. Schroeder, K. Martin, and B. Lorensen. *The Visualization Toolkit: An Object-Oriented Approach to 3D Graphics*. Prentice Hall PTR, New Jersey, 1996.
- [34] Surgical Planning Laboratory Web Site. <http://www.spl.harvard.edu>.
- [35] O. Skrinjar and J. S. Duncan. Real time 3D brain shift compensation. In *Proceedings of International Conference of Information Processing in Medical Imaging*, pages 641–649, 1999.
- [36] O. Skrinjar, C. Studholme, A. Nabavi, and J. Duncan. Steps Toward a Stereo-Camera-Guided Biomechanical Model for Brain Shift Compensation. In *Proceedings of International Conference of Information Processing in Medical Imaging*, pages 183–189, 2001.
- [37] M. Sonka and J. Fitzpatrick. *Handbook of Medical Imaging*, volume 2. SPIE Publications, Bellingham, Washington, USA, 2000.
- [38] S. L. Talagala, C. A. Jungreis, E. Kanal, S. P. Meyers, T. K. Foo, R. A. Rubin, and G. R. Applegate. Fast Three-Dimensional Time of Flight MR Angiography of the Intra-Cranial Vasculature. *Journal of Magnetic Resonance Imaging*, 5:317–323, 1995.
- [39] A. Tei, F. Talos, A. Bharatha, M. Ferrant, P. McL. Black, F. A. Jolesz, R. Kikinis, and S. K. Warfield. Tracking Volumetric Brain Deformation During Image Guided Neurosurgery. In *VISIM: Information Retrieval and Exploration in Large Medical Image Collections, in conjunction with MICCAI 2001: the Fourth International Conference on Medical Image Computing and Computer Assisted*

*Intervention; 2001 Oct 14–17; Utrecht, the Netherlands, Heidelberg, Germany, 2001. Springer-Verlag.*

- [40] T. Ting. *Anisotropic elasticity: theory and Applications*. Oxford University Press, 1996.
- [41] S. K. Warfield, M. Ferrant, X. Gallez, A. Nabavi, F. A. Jolesz, and R. Kikinis. Real-Time Biomechanical Simulation of Volumetric Brain Deformation for Image Guided Neurosurgery. In *SC 2000: High Performance Networking and Computing Conference; 2000 Nov 4–10; Dallas, USA*, pages 230:1–16, 2000.
- [42] S. K. Warfield, A. Guimond, A. Roche, A. Bharatha, A. Tei, F. Talos, J. Rexilius, J. Ruiz-Alzola, C. Westin, S. Haker, S. Angenent, A. Tannenbaum, F. A. Jolesz, and R. Kikinis. Advanced Nonrigid Registration Algorithms for Image Fusion. In Arthur W. Toga, editor, *Brain Mapping: The Methods*, page To Appear. San Diego, USA: Academic Press, 2nd edition.
- [43] S. K. Warfield, F. Jolesz, and R. Kikinis. A High Performance Computing Approach to the Registration of Medical Imaging Data. *Parallel Computing*, 24:1345–1368, 1998.
- [44] S. K. Warfield, A. Nabavi, T. Butz, K. Tuncali, S. G. Silverman, P. McL. Black, F. A. Jolesz, and R. Kikinis. Intraoperative Segmentation and Nonrigid Registration For Image Guided Therapy. In *MICCAI 2000: Third International Conference on Medical Robotics, Imaging And Computer Assisted Surgery; 2000 Oct 11–14; Pittsburgh, USA*, pages 176–185, Heidelberg, Germany, 2000. Springer-Verlag.
- [45] S. K. Warfield, F. Talos, A. Tei, A. Bharatha, A. Nabavi, M. Ferrant, P. McL. Black, F. A. Jolesz, and R. Kikinis. Real-Time Registration of Volumetric Brain MRI by Biomechanical Simulation of Deformation during Image Guided Neurosurgery. *Computing and Visualization in Science*. In Press.



- [46] W. M. Wells, P. Viola, H. Atsumi, S. Nakajima, and R. Kikinis. Multi-modal volume registration by maximization of mutual information. *Medical Image Analysis*, 1:35–51, 1996.
- [47] C. Westin, L. Wigstrom, T. Looock, L. Sjoqvist, R. Kikinis, and H. Knutsson. Three-Dimensional Adaptive Filtering in Magnetic Resonance Angiography. *Journal of Magnetic Resonance Imaging*, 14:63–71, 2001.
- [48] A. Yezzi, A. Tsai, and A. Willsky. Medical image segmentation via coupled curve evolution equations with global constraints. In *Mathematical Methods in Biomedical Image Analysis*, pages 12–19, 2000.
- [49] O. Zienkewickz and R. M. Taylor. *The Finite Element Method*, volume 4th Edition. McGraw Hill Book Co., New York, 1987.